Research Paper

GEOSPHERE

GEOSPHERE; v. 13, no. 2

doi:10.1130/GES01433.1

5 figures; 2 plates; 4 tables; 1 supplemental file

CORRESPONDENCE: ryan.b.anderson@wsu.edu

CITATION: Anderson, R.B., Long, S.P., Horton, B.K., Calle, A.Z., and Ramirez, V., 2017, Shortening and structural architecture of the Andean fold-thrust belt of southern Bolivia (21°S): Implications for kinematic development and crustal thickening of the central Andes: Geosphere, v. 13, no. 2, doi:10.1130/GES01433.1.

Received 22 September 2016
Revision received 28 November 2016
Accepted 24 January 2017

Shortening and structural architecture of the Andean fold-thrust belt of southern Bolivia (21°S): Implications for kinematic development and crustal thickening of the central Andes

Ryan B. Anderson[1], Sean P. Long[1], Brian K. Horton[2], Amanda Z. Calle[2], and Victor Ramirez[3]

[1]School of the Environment, Washington State University, PO Box 642812, Pullman, Washington 99164, USA
[2]Department of Geological Sciences and Institute for Geophysics, Jackson School of Geosciences, 2275 Speedway Stop C9000, University of Texas, Austin, Texas 78712, USA
[3]Instituto de Investigaciones Geológicas y del Medio Ambiente, Universidad Mayor de San Andrés, Calle 27 Cota Cota, La Paz, Bolivia

ABSTRACT

Reliable crustal shortening estimates for the central Andes (South America) are a critical component in validating models of Cordilleran processes. In southern Bolivia, insight into crustal shortening and the kinematic development of the Andean thrust belt are limited by the lack of a unified structural evaluation across the entire width of the retroarc region. To address these shortcomings, we (1) estimate crustal shortening by integrating new geologic mapping with published geophysical data to construct a balanced cross section across the Subandean zone (SAZ), Interandean zone (IAZ), and Eastern Cordillera (EC) at 21°S; (2) develop a kinematic model for the retroarc thrust belt; and (3) estimate crustal budgets and average crustal thicknesses over the region. We estimate 337 ± 69 km (36% ± 7%) of total shortening (SAZ, 82 km; IAZ, 70 km; EC, 120 km; Altiplano, 65 km). The thrust belt developed from late Eocene time to the present by tectonic wedging and eastward emplacement of two ~10–12-km-thick basement thrust sheets that distribute slip into overlying sedimentary rocks. Our range of crustal shortening values can account for 90%–118% of the current retroarc crustal area. Assuming an initial crustal thickness of 35 km, the EC and Altiplano did not achieve modern crustal thicknesses (~65 km) until the present. However, assuming a 40-km-thick initial crust, the EC and Altiplano attained the critical thickness for either eclogitic phase changes or lower crustal flow (>45–50 km) by ca. 27–25 Ma, modern thicknesses by ca. 10 Ma, and currently exceed geophysically observed thicknesses by ~2.5–14.5 km; this suggests crustal losses significant enough to have affected hinterland surface elevation.

INTRODUCTION

The ~7000-km-long Andean orogen of South America is the type example of an active continental margin orogenic system, and the central Andes have emerged as a focal point in debates over multiple orogenic processes (e.g., Oncken et al., 2006; DeCelles et al., 2015). In cordilleran-style orogenic belts, primary features observed in the overriding continental plate (e.g., deformation, topographic growth, magmatism, synorogenic sedimentation) are attributed to a diverse array of geodynamic processes, including the dynamics of plate convergence and properties of the subducting oceanic slab (e.g., Pardo-Casas and Molnar, 1987; Coney and Evenchick, 1994; Gephart, 1994; Lallemand et al., 2005), processes operating within the mantle lithosphere such as thermal weakening, mantle flux, and delamination of dense lithospheric roots (e.g., Isacks, 1988; Allmendinger et al., 1997; Lamb and Hoke, 1997; Ducea, 2001; DeCelles et al., 2009), or erosional modification of the orogenic wedge due to climatic variations (e.g., Horton, 1999; Willett, 1999; Montgomery et al., 2001; Sobel et al., 2003; McQuarrie et al., 2008a). Commonly the record of such processes is only preserved in the overriding plate. Geologic mapping and balanced cross sections provide an important framework within which to analyze the mechanisms of orogenesis because they provide plausible constraints on the geometry, kinematics, and magnitude of shortening, which are fundamental parameters for quantifying deformation rates and crustal thickness budgets (e.g., Sheffels, 1990; Kley, 1996; Kley and Monaldi, 1998; McQuarrie, 2002; Gotberg et al., 2010; Eichelberger et al., 2015).

In southern Bolivia (21°S; Fig. 1), efforts to understand processes operating within the central Andes are hindered by variable and uncertain published shortening magnitudes; this precludes assessment of how deformation in the thrust belt may be linked to differing geodynamic models. At this latitude, the retroarc thrust belt contains one of the best exposed stratigraphic sections in the central Andes (Sempere, 1995; Horton et al., 2001), is one of the few locations where hinterland intermontane basins preserve a record of Eocene to Miocene deformation (Horton, 1998), and is the site of published geophysical data sets that extensively characterize lithospheric-scale structure (e.g., Götze et al., 1994; Wigger et al., 1994; Schmitz and Kley, 1997; Beck and Zandt, 2002), making it an ideal location to illustrate deformation geometry and quantify crustal shortening. However, a regional cross section through the entire retroarc at 21°S is currently lacking. Current kinematic interpretations and shortening estimates rely on a composite of published cross sections from individual tectonomorphic zones, resulting in inconsistent shortening magnitudes

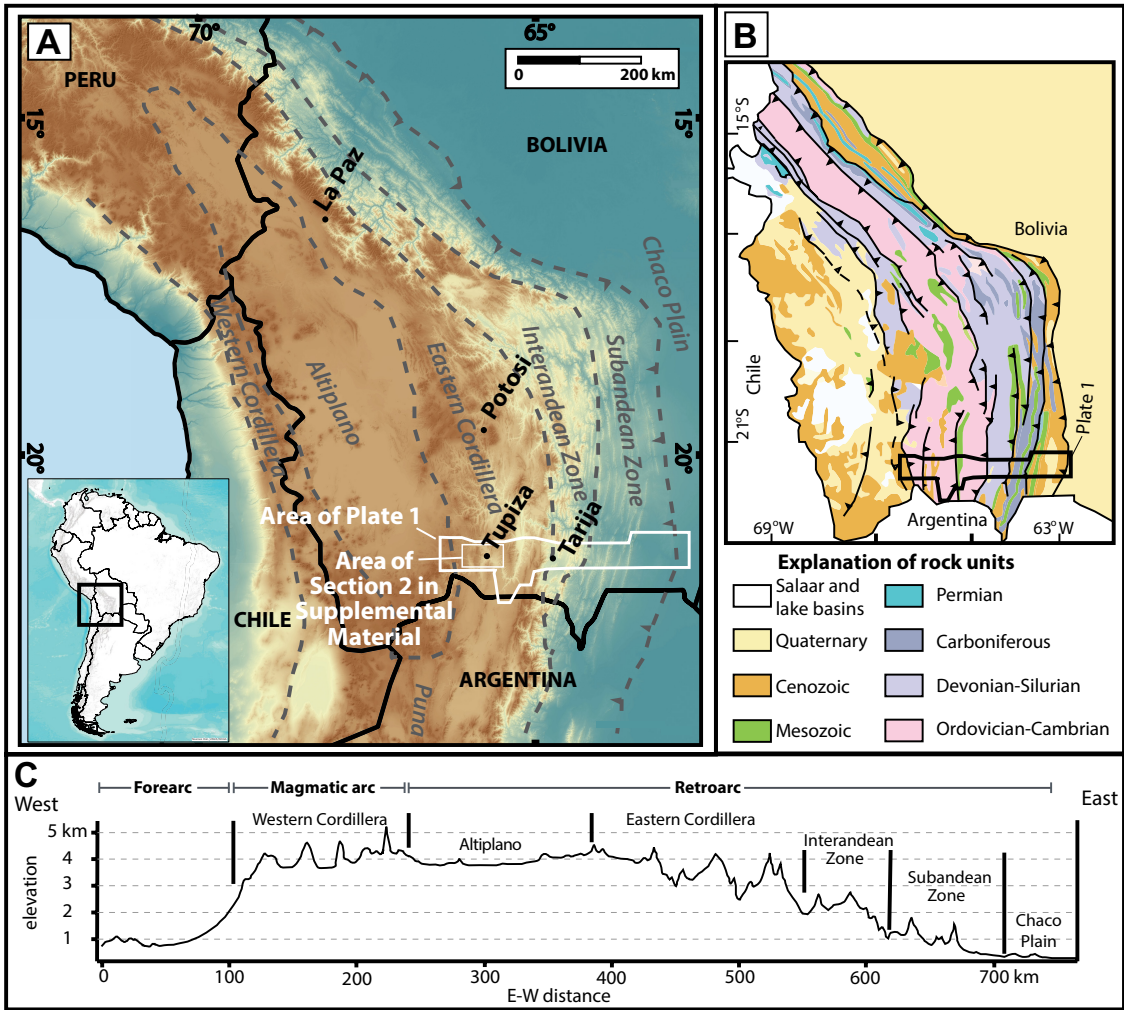

Figure 1. (A) Topography of the central Andes (constructed from a Shuttle Radar Topography Mission 90 m digital elevation model); dashed gray lines mark the boundaries of tectonomorphic zones. Locations of Plate 1 and Figure SM2 (see footnote 1) are denoted by white boxes. (B) Generalized geology of Bolivia; black box denotes location of Plate 1 (modified from McQuarrie, 2002; Eichelberger et al., 2013). (C) Topographic profile of the central Andes at 21°S from the Chilean coast to the Chaco plain. Profile emphasizes topographic steps between the tectonomorphic zones.

(199–320 km) (Dunn et al., 1995; Kley, 1996; Baby et al., 1997; Müller et al., 2002; Elger et al., 2005; Oncken et al., 2006), and differing interpretations of how basement deformation is linked to deformation in the overlying sedimentary cover sequence (e.g., Baby et al., 1997; Müller et al., 2002; McQuarrie, 2002).

Recent paleoaltimetry data sets at ~21°S suggest rapid surface uplift (~2–3 km) of the Altiplano and Eastern Cordillera in the middle-late Miocene has been attributed to rapid removal of dense, eclogitic lower crust and mantle lithosphere (Sobolev and Babeyko, 2005; Garzione et al., 2006, 2014; Ghosh et al., 2006; Molnar and Garzione, 2007; Hoke and Garzione, 2008; Cadena et al., 2015; Wang et al., 2015). In addition, delamination-related magmatism and the felsic composition of the 60–70-km-thick crust below the southern Altiplano suggest that loss of lower crust has occurred in the central Andes (Kay and Kay, 1993; Beck and Zandt, 2002). However, a longstanding debate regarding the central Andes has focused on whether shortening can fully account for the observed 60–70-km-thick crust in the Altiplano, because many early shortening estimates could only account for 70%–80% of the observed crustal

area (Sheffels, 1990; Kley, 1996; Allmendinger et al., 1997; Baby et al., 1997; Kley and Monaldi, 1998; McQuarrie, 2002; Gotberg et al., 2010). Recent orogen-scale cross sections, map-view and paleomagnetic rotation reconstructions, and foreland basin studies interpret that crustal shortening and accompanying underthrusting of foreland lithosphere are sufficient to account for the crustal area of the Andes between 15° and 22°S (Kley, 1999; McQuarrie and DeCelles, 2001; McQuarrie, 2002; DeCelles and Horton, 2003; McQuarrie et al., 2005; Hindle et al., 2005; Arriagada et al., 2008; Eichelberger and McQuarrie, 2015; Eichelberger et al., 2015). However, the wide range of existing shortening estimates still falls short of accounting for crustal area at 21°S (Kley and Monaldi, 1998). Given the current debates over the links between shortening, delamination, and surface uplift, the uncertain shortening magnitude at this latitude calls for reassessment of the crustal thickness budget. Such a study would provide a benchmark for understanding if there was sufficient excess material available for removal that would significantly affect surface elevations. In addition, a structural analysis across the entire backarc in southern Bolivia would provide key context for validating other geodynamic models in the central Andes, such as oroclinal development (e.g., Eichelberger and McQuarrie, 2015) or testing proposed links between several primary cordilleran processes (e.g., DeCelles et al., 2009).

To address these problems we incorporate new geologic mapping with published geophysical data to construct a regional cross section that encompasses the entire Bolivian retroarc at 21°S. This allows us to calculate a comprehensive estimate of crustal shortening, present a new kinematic model for thrust belt development, assess upper and lower bounds for the crustal thickness budget, and calculate constraints on the average crustal thickness during thrust belt construction.

GEOLOGIC SETTING

Late Cretaceous–Cenozoic construction of the Andean orogen has been marked by progressive crustal thickening, magmatic arc development, and eastward advance of a retroarc fold-thrust belt and foreland basin system within the South American continental plate (Coney and Evenchick, 1994; Sempere et al., 1997; Horton and DeCelles, 1997; DeCelles and Horton, 2003; McQuarrie et al., 2005). The central Andes (~16°–24 °S) are the widest part of the orogen, and have accommodated the greatest amount of crustal shortening (e.g., McQuarrie, 2002).

The central Andean retroarc has been divided into five tectonomorphic zones that are defined by major steps in mean topographic and structural elevation (Fig. 1; Kley, 1996; McQuarrie, 2002). From west to east, they include the hinterland plateau, the Altiplano, a broad fold-thrust belt that has been divided into the Eastern Cordillera (EC), Interandean zone (IAZ), and Subandean zone (SAZ), and the modern foreland basin, the Chaco plain. The Altiplano is a high-elevation, low-relief, internally drained basin bordered on the west by the Western Cordillera (the modern volcanic arc) and on the east by the EC (Isacks, 1988; Allmendinger et al., 1997; McQuarrie, 2002). The EC is the structurally highest part of the thrust belt, elevated relative to the adjacent Altiplano and IAZ. The EC is bivergent, characterized by west-vergent backthrusts in the west and east-vergent forethrusts in the east (McQuarrie and DeCelles, 2001; McQuarrie, 2002; Müller et al., 2002). Major changes in structural elevation between the EC and IAZ, and IAZ and SAZ, are interpreted as the result of the emplacement and passage of concealed basement megathrust sheets over crustal-scale footwall ramps (e.g., Kley et al., 1996; McQuarrie, 2002; Müller et al., 2002). The IAZ is a narrow transitional zone of intermediate structural and topographic levels between the EC and SAZ (Kley, 1996), and the SAZ encompasses the foothills of the eastern Andes (Dunn et al., 1995; Uba et al., 2009). Both the IAZ and SAZ are characterized as primarily east-vergent thrust systems detached from a basal décollement in Silurian shale (Baby et al., 1992; Dunn et al., 1995; Moretti et al., 1996; Kley, 1996). The modern foreland basin system is located in the Chaco plain, east of the Andean topographic front (Horton and DeCelles, 1997).

Orogenesis of the central Andes initiated and was likely focused along the western margin of the South American continent from the Late Cretaceous to mid-Paleogene (ca. 70–45 Ma) (e.g., Horton and DeCelles, 1997; Sempere et al., 1997; McQuarrie et al., 2005). The thrust front made a major eastward advance (~400 km) to the EC by ca. 40 Ma (Horton, 2005; Elger et al., 2005; Ege et al., 2007), and has continued to propagate eastward to its present position in the Chaco plain (Horton and DeCelles, 1997; Brooks et al., 2011).

METHODS

Geologic Mapping

This study presents new geologic mapping at scales of 1:50,000 and 1:24,000, and is displayed in Plate 1 (scale 1:200,000). Mapping was conducted on 1:50,000 Instituto Geografico Militar Bolivia topographic base maps (retrieved from http://www.igmbolivia.gob.bo/), and 1:24,000 Bing Maps aerial imagery overlain with a 20 m topographic contour interval. Mapping was focused between 21°10′S and 22°10′S along an ~300 km east-west transect from the Chaco plain to the eastern Altiplano. Map data were collected principally on the roads from Villamontes to Tarija, Tarija to Tupiza, and Tupiza to San Vincente, with several ancillary transects near Tarija and Tupiza (see Plate 1 for locations of transect routes). In the Chaco plain, seismic reflection profiles tied to well logs from Uba et al. (2009) were extrapolated to the surface. In addition, the new mapping was integrated with published geologic maps (Servicio Geologico de Bolivia, 1992; Horton, 1998; Müller et al., 2002; Servicio Nacional de Geologica y Tecnico de Minas, 2009, 2010). ArcGIS software (https://www.arcgis.com/) was used for compilation of published maps and digitization of field sheets. Stratigraphic and structural contacts were extended along strike using a combination of topographic maps, aerial imagery, and published geologic maps.

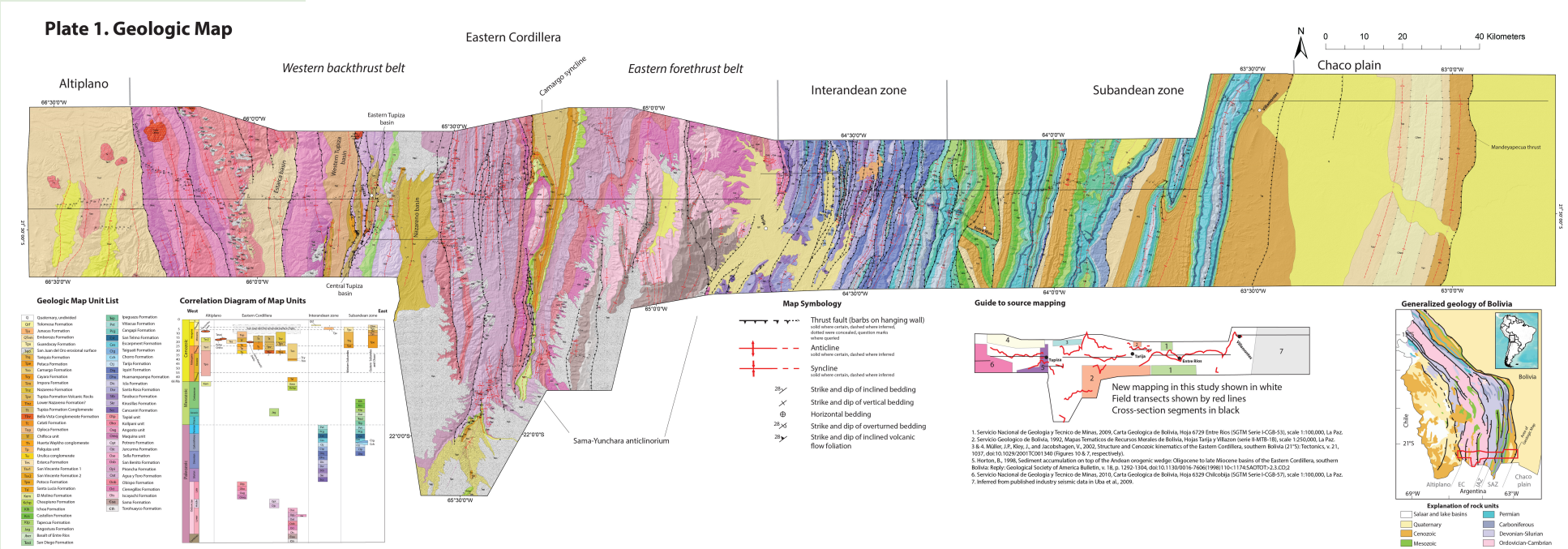

Plate 1. Geologic map of the Andean retroarc (Eastern Cordillera, Interandean zone, Subandean zone) between ~21°45′S and 22°0′S, with a list of geologic units, correlation chart of map units, guide to compiled published maps, and a reference map showing mapping transects in this study. Scale is 1:200,000. To view Plate 1 at full size, please visit http://doi.org/10.1130/GES01433.S1 or the full-text article on www.gsapubs.org.

Balanced Cross Section

A balanced cross section, oriented perpendicular to the regional strike of thrust faults and folds, was constructed based on field data projected from east-west mapping traverses. Deformed and restored sections were hand-drafted using line-length balancing methods (e.g., Dahlstrom, 1969; Elliott, 1983), and are both displayed at 1:200,000 scale (Plate 2). Across-strike stratigraphic variation and near-surface geometry are obtained from apparent dips calculated from our mapping, and the manner in which the space above the basal décollement of the thrust belt is filled was supplemented by available published stratigraphic and geophysical constraints (e.g., Woodward et al., 1989; McQuarrie et al., 2008b). The final line-length balanced section was compared to an area-balanced cross section to ensure that shortening estimates were reliable, and to quantify total shortening uncertainties (e.g., Judge and Allmendinger, 2011; Allmendinger and Judge, 2013). Detailed justifications for individual drafting decisions on the cross section are annotated in Plate 2. More detailed discussions of the methods of cross section construction and the assessment of the uncertainty are found in the Supplementary Material[1].

STRATIGRAPHY

The stratigraphic section observed along the mapped transect consists of an ~10–15-km-thick package of predominantly siliciclastic sedimentary rocks ranging in age from Cambrian to Quaternary (Sempere, 1995; Tankard et al., 1995; Welsink et al., 1995). However, significant along- and across-strike variations in the stratigraphic thicknesses of Paleozoic–Mesozoic rocks (Plate 2), as well as regional erosional unconformities, are observed across the thrust belt, and are interpreted as a result of pre-Andean tectonism (Sempere, 1995; Tankard et al., 1995). Because formation names vary regionally, stratigraphic units are described here based on formation age. A detailed stratigraphic correlation chart with individual unit names can be found in Plate 1 and Figure 2.

In southern Bolivia, the Chaco plain, SAZ, and IAZ deform an ~10–12-km-thick section of Silurian to Cenozoic clastic sedimentary rocks (Fig. 2; Baby et al., 1992; Dunn et al., 1995; Sempere, 1995). Gravimetric modeling indicates that Silurian rocks overlie crystalline basement, rather than the thick sedimentary section of Ordovician and Cambrian rocks observed to the west in the EC (Fig. 2; Plate 2; Kley et al., 1996; Schmitz and Kley, 1997). Across-strike thickness trends of Silurian rocks at 21°S are not precisely known because

1 **Supplementary material for: Shortening and structural architecture of the**
2 **Andean fold-thrust belt of southern Bolivia (21°S): Implications for kinematic**
3 **development and crustal thickening of the central Andes**
4
5 **SECTION SM1: BALANCED CROSS SECTION METHODS**
6 The balanced cross section was constructed based on field data projected from east-
7 west mapping traverses, which are oriented perpendicular to the regional strike of thrust faults
8 and folds (Plate 2). Because field data could not be collected in an uninterrupted east-west
9 transect, map data were projected from six across-strike traverse segments. Each segment
10 contains a high density of field measurements, and segment breaks were placed at stratigraphic
11 or structural contacts that are continuous along strike (Plate 1). On Plate 2, the deformed and
12 corresponding restored cross sections are both displayed at 1:200,000 -scale.

[1]Supplemental Material. Detailed balanced cross-section methodology and estimation of uncertainty, structural reinterpretation, and sequential restoration of the Tupiza region. Please visit http://doi.org/10.1130/GES01433.S3 or the full-text article on www.gsapubs.org to view the Supplemental Material.

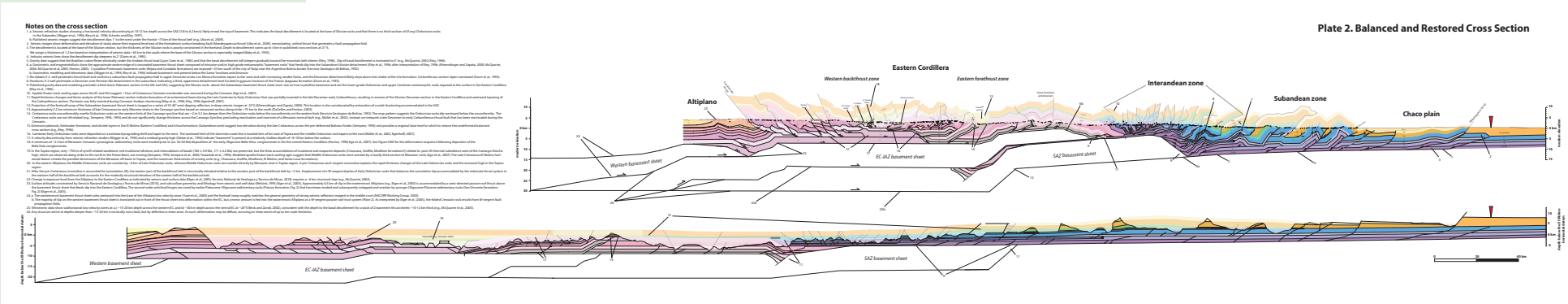

Plate 2. Line-length balanced deformed and restored cross sections based on geologic mapping from Plate 1, with detailed annotations of individual drafting decisions on the cross section. Scale is 1:200,000. To view Plate 2 at full size, please visit http://doi.org/10.1130/GES01433.S2 or the full-text article on www.gsapubs.org.

a complete section is only exposed in one location in the IAZ (Plate 1), and the base of the Silurian section is poorly imaged under the Chaco plain (Baby et al., 1992; Dunn et al., 1995). However, Silurian rocks are exposed across the SAZ, IAZ, and EC in central and northern Bolivia, and gently thicken westward (McQuarrie, 2002; Eichelberger et al., 2013). Silurian rocks at 21°S are therefore assumed to thicken westward from ~1.2 km in the Chaco plain (Baby et al., 1992) to ~1.6 km in the IAZ (Plate 2). Due to extensive surface exposures across the SAZ and IAZ (Plate 1), and well control and seismic data in the Chaco plain (e.g., Baby et al., 1992; Dunn et al., 1995; Uba et al., 2006, 2009), the thicknesses of Devonian through Cenozoic rocks are well constrained. The Devonian section maintains a thickness of ~2.8 km across the Chaco plain and eastern SAZ, but thins westward to ~1.5 km at the IAZ-SAZ boundary. The Carboniferous section thins westward, from ~2.2–2.4 km in the Chaco plain and eastern SAZ (Baby et al., 1992; Dunn et al., 1995), to ~1.5 km in the central SAZ, to ~0.5 km at the IAZ-EC boundary (Plate 2). Permian rocks are ~0.6 km thick across the Chaco plain, SAZ, and IAZ.

Triassic red beds and Jurassic basalts (Sempere, 1995; Bertrand et al., 2014) vary between 200 and 500 m thick, and are restricted to the western SAZ. Overlying Jurassic and Cretaceous rocks thicken from tens of meters in the Chaco plain (Uba et al., 2009) and eastern SAZ to ~1.5 km in the central and western SAZ (Plate 2). As much as ~4.3 km of Cenozoic synorogenic sedimentary rocks are preserved along the transect (Plate 2), and record the eastward advance of the Andean foreland basin across the SAZ and Chaco plain from ca. 27 Ma to the present (Horton and DeCelles, 1997; Echavarria et al., 2003; Uba et al., 2009; Hulka and Heubeck, 2010). No Cenozoic rocks are preserved in the IAZ, but Cenozoic apatite fission track (AFT) ages obtained there suggest that at least ~3.0 km of Mesozoic–Cenozoic overburden was present prior to the onset of Andean deformation ca. 25–12 Ma, but has since been eroded (Ege et al., 2007).

The stratigraphy of the EC is characterized by a >10-km-thick section of upper Cambrian to Ordovician, low-grade (epizone-anchizone) metasedimentary rocks (Jacobshagen et al., 2002), which are unconformably overlain by narrow, north-south–trending outcrop belts of unmetamorphosed Cretaceous and Cenozoic rocks, which in turn are beveled by the Miocene–Pliocene San Juan del Oro erosional surface (Plate 1; Fig. 2) (Gubbels et al., 1993; Kennan et al., 1995, 1997; Horton, 1998, 2005; Müller et al., 2002; DeCelles and Horton, 2003). Early Paleozoic tectonism (Egenhoff, 2007) and a Late Devonian to Carboniferous orogenic event (Sempere, 1995; Jacobshagen et al., 2002) resulted in significant variation in Paleozoic stratigraphic thicknesses across the EC-IAZ boundary (Plate 2; Kley, 1996). In particular, the ~4.3-km-thick section of Silurian–Permian rocks at the IAZ-EC boundary is not observed in the hinge zone of the Camargo syncline ~50 km to the west, where Mesozoic–Cenozoic rocks unconformably overlie Ordovician rocks (Plate 1). Cambrian–Early Ordovician rocks thin to the west and Middle and Late Ordovician rocks thin to the east (Egenhoff, 2007). Early–Middle Ordovician rocks are not exposed west of Tupiza (Plate 1), but a velocity discontinuity at ~8–10 km interpreted as the basement-cover contact (Wigger et al., 1994; Schmitz and Kley, 1997) coupled with the known thicknesses of overlying Late Ordovician rocks yields a thickness estimate of ~5 km for Early–Middle Ordovician rocks in the subsurface of the western EC (Plate 2, annotation 17).

The Mesozoic–Cenozoic rocks of the EC are differentiated into separate western (Tupiza region; see detailed discussion in Supplementary Material, and Figs. SM1, SM2 [footnote 1]) and eastern (Camargo syncline; Plate 1) outcrop belts based on contrasting sediment dispersal patterns, depositional setting, and lithology (Sempere, 1994; Sempere et al., 1997; Horton, 1998, 2005; DeCelles and Horton, 2003). Nearly ~700 m of distinctive upper Cretaceous to Paleocene restricted marine rocks with pervasive paleosol development are preserved in the Camargo syncline, and directly overlie Ordovician rocks (Plate 1). These strata (El Molino Formation, Fig. 2) are significant as they are correlative throughout the central Andes, and reflect regionally extensive low topography prior to Andean deformation (Sempere, 1994; Welsink et al., 1995; Sempere et al., 1997; Horton et al., 2001). Overlying Cenozoic rocks preserve an ~2.5-km-thick Paleogene foredeep section (DeCelles and Horton, 2003; Horton, 2005).

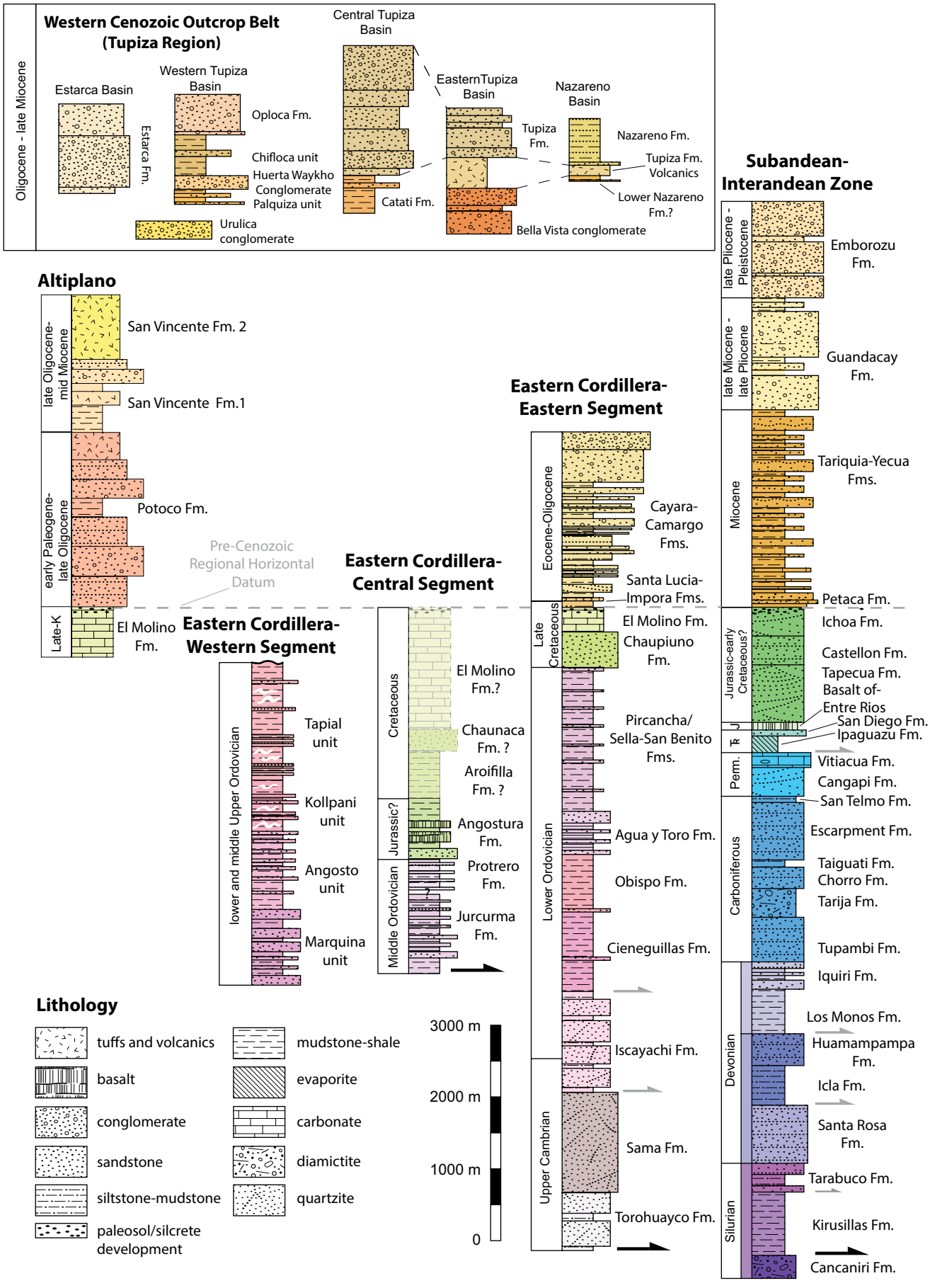

Figure 2. Stratigraphic column of the southern central Andes of Bolivia (modified from Dunn et al., 1995; Sempere, 1995; Welsink et al., 1995; Horton, 1998; Müller et al., 2002; DeCelles and Horton, 2003; Uba et al., 2006; Elger et al., 2005; Egenhoff, 2007). Columns across the tectonomorphic zones are restored to a pre-Cenozoic horizontal datum defined by regionally correlative upper Cretaceous paleosols and silcretes (e.g., Kley, 1996). Black and gray arrows indicate the major and minor (respectively) décollement horizons across the thrust belt. Colors correspond with formation age divisions used for the cross-section line (Plate 2). See Plate 1 for the complete map unit list and correlation diagram.

In the western Cenozoic outcrop belt, late Oligocene AFT ages suggest erosion of ≥3 km of Mesozoic–Cenozoic rocks, followed by Oligocene to late Miocene intermontane basin development (Horton, 1998, 2005; Müller et al., 2002; Ege et al., 2007). Near Tupiza (Fig. 1), an ~750-m-thick section of Cretaceous sandstone, mudstone, siltstone, and interlayered basalt is preserved in a narrow north-south–trending syncline (Sempere et al., 2002), but the distinctive upper Cretaceous to Paleocene El Molino Formation is only present as recycled clasts within Cenozoic synorogenic sedimentary rocks (Horton, 1998). After erosion of the Paleogene foredeep section, between ~0.6 and 2.3 km of sedimentary and volcanic rocks (Fig. 2) were deposited across 5 separate basins (Nazareno, Eastern Tupiza, Central Tupiza, Western Tupiza, and Estarca basins; Plate 1; Fig. SM2) during the Oligocene to late Miocene (Hérail et al., 1996; Horton, 1998; Müller et al., 2002). The San Juan del Oro erosional surface is a broad erosional pediment developed between ca. 12 and 3 Ma that beveled deformed Paleozoic to Cenozoic rocks and signified the end of major deformation in the EC (Gubbels et al., 1993; Kennan et al., 1995, 1997).

In the easternmost Altiplano, nearly 4 km of Cenozoic synorogenic sedimentary and volcanic rocks overlie the upper Cretaceous–Paleocene El Molino Formation (Fig. 2; Welsink et al., 1995; Elger et al., 2005; Servicio Nacional de Geologica y Tecnico de Minas, 2010).

STRUCTURAL ZONES

In the following we describe, from east to west, the map patterns, structural style, and deformation geometry of each tectonomorphic zone of the Andean fold-thrust belt, as determined from our new mapping (Plate 1) and balanced cross section (Plate 2).

Chaco Plain

The western Chaco plain comprises the wedge-top portion of the modern Andean foreland basin system and encompasses the region between the main topographic front to the frontal-most thrust ~60 km to the east (Tankard et al., 1995; Moretti et al., 1996; Horton and DeCelles, 1997; Uba et al., 2006, 2009). Surface exposures consist of Neogene synorogenic sedimentary rocks and Quaternary sediment (Plate 1). One prominent feature is a north-trending exposure of gently folded Neogene sedimentary rocks in the hanging wall of the surface-breaching Mandeyapecua thrust, which marks the deformation front of the thrust belt. It is debated how much active shortening is distributed on the Mandeyapecua thrust (e.g., Mugnier et al., 2006; Brooks et al., 2011; Yagupsky et al., 2014), but the trace of the gentle topographic ridge associated with the fault is continuous along strike from ~18° to 22°S and shows some evidence of Quaternary rupture (Costa et al., 2006; Brooks et al., 2011).

In the Chaco plain, the basal décollement is located within shales near the base of the Silurian section (Baby et al., 1992; Dunn et al., 1995). Based on seismic reflection data ~65 km to the south (Baby et al., 1992), we assign a 10 km depth to décollement at the eastern limit of the cross section (see Plate 2, annotation 3, and discussion of uncertainty in Supplementary Material [footnote 1]). Seismic reflection data tied to well logs also constrain a 1°–2° west dip for the basal décollement (Baby et al., 1992; Dunn et al., 1995; Moretti et al., 1996; Uba et al., 2006, 2009).

The subsurface structure of the Chaco plain is characterized by gentle (5°–15° limb dips) fault-propagation folds above east-vergent, low-offset (~1–4.5 km) thrust faults that ramp up from the basal décollement (Plate 2). However, the Mandeyapecua thrust is an emergent thrust with a hanging-wall syncline-anticline geometry produced from fault-bend folding above a multibend thrust fault. In the footwall of the Mandeyapecua thrust, Devonian–Silurian rocks are folded and overlying Carboniferous–Cenozoic rocks are elevated above their regional level (e.g., Uba et al., 2009), suggesting the presence of a concealed thrust that tips out within the Carboniferous section ~10 km east of the emergent thrust front (Plate 2). Sedimentological and geochronologic data record arrival and unsteady advance of the deformation front in the Chaco plain by ca. 5.9 Ma, followed by westward retreat of deformation to the SAZ between ca. 4.0 and 2.1 Ma, and refocusing of the deformation front at the Mandeyapecua thrust since ca. 1.5 Ma (Uba et al., 2009).

Subandean Zone

The SAZ is defined by a Valley-and-Ridge–style topography characterized by anticlinal ranges separated by synclinal valleys, which are continuous for hundreds of kilometers along strike (Fig. 1; Plate 1). Folds and thrust faults are east vergent, with an overall north-northeast–trending (~005°–020°) structural grain (Plate 1). Folds generally exhibit broad wavelengths (5–10 km), with Carboniferous to Cretaceous rocks exposed in the cores of anticlines and extensive exposures of Neogene synorogenic sedimentary rocks in the hinges of intervening synclines.

Teleseismic data image a subhorizontal velocity discontinuity at ~10–12 km depth across the SAZ, which is interpreted as the contact between Silurian sedimentary rocks and denser basement (Wigger et al., 1994). This is consistent with an interpreted 1°–2° west dip for the basal décollement projected westward from the Chaco plain under the SAZ (Plate 2, annotation 1; Dunn et al., 1995). The anticlinal ranges of the eastern SAZ are narrow in width and structurally simple, with smaller offset (~5–7 km) thrust faults branching off the basal décollement, breaching the cores of several anticlines as a result of progressive growth of fault-propagation folds. In the western SAZ, large-scale fault-bend folding of thrust sheets occurs as larger offset (~8–20 km) thrust faults cut upsection from the Silurian décollement to secondary detachment levels in Devonian shale and Triassic evaporites (Plate 2, annotations 7–8; Dunn et al., 1995).

In map view, the SAZ-IAZ boundary is demarcated by a westward transition to thin, closely spaced (~2–3 km) thrust sheets that carry upper Devonian to Carboniferous rocks, indicating an increase in structural level. In addition, the widely spaced Valley-and-Ridge topography of the SAZ gives way to more closely spaced, sharp-crested ranges separated by deeply incised valleys, with a gradual westward increase in elevation (Fig. 1). The basal décollement under

the western SAZ is inferred to gradually steepen toward the mountain belt interior due to loading and flexure of the underthrusted Brazilian shield (Lyon-Caen et al., 1985). The dip of the décollement increases to 4° (e.g., McQuarrie, 2002) at approximately the SAZ-IAZ boundary, where the elevated structural level implies increased loading on the underlying Brazilian shield (Plate 2, annotation 5). A dramatic increase in the sedimentation rates of synorogenic rocks in the western SAZ beginning ca. 12–8 Ma is interpreted as the result of enhanced crustal flexure induced by the approaching deformation front, and is inferred to be the time frame for the onset of SAZ deformation (Echavarria et al., 2003; Uba et al., 2009).

Interandean Zone

In the IAZ, the structural grain has a dominant north-northeast (~005°–020°) trend, and faults and fold axes are more closely spaced (1–3 km). The western half of the IAZ is deformed into an imbricate stack of dominantly west-vergent thrust faults, whereas the eastern IAZ is deformed into an imbricate stack of dominantly east-vergent thrust faults (Plate 2). The stratigraphic exposure level changes from the SAZ to the IAZ, and is dominated by Devonian and Silurian rocks (Plate 1). The deepest stratigraphic levels are exhumed in the central IAZ, where the change in vergence direction produced a structurally complex synformal klippe (Plate 2).

Across the IAZ, the basal levels of tightly folded synclines containing Carboniferous rocks define a regional structural level that suggests a horizontal décollement at a relatively shallow depth (~5–6 km) (Plate 2; Kley et al., 1996). Upper Silurian rocks are the deepest exposed rocks in the IAZ (Plate 1), and the décollement under the IAZ is therefore interpreted to be located within the same Silurian stratigraphic horizon as the basal SAZ décollement. On the basis of the known stratigraphic thickness of the Paleozoic section from surface data (Fig. 2), the décollement in the IAZ is elevated ~11 km relative to the basal décollement in the western SAZ (Plate 2). The increase in structural elevation at the IAZ-SAZ boundary is also coincident with the eastern edge of a residual Bouguer gravity anomaly and a lateral change in the velocity structure of the upper crust (Plate 2, annotation 12; Wigger et al., 1994; Kley et al., 1996; Schmitz and Kley, 1997). Such a regional change in exposure level requires the presence of a major footwall or hanging-wall ramp, and the filling of space below the elevated Silurian décollement in the IAZ can be accomplished in two end-member scenarios: (1) structural repetition of Silurian–Neogene sedimentary rocks, thereby doubling the structural thickness of the section, or (2) by emplacement of a thick thrust sheet of pre-Silurian basement rocks (Kley et al., 1996; Dunn et al., 1995; McQuarrie, 2002). Gravimetric modeling and velocity models from teleseismic data favor the latter, and the gravity data suggest density values typical of true crystalline basement and not the Ordovician–Cambrian metasedimentary rocks observed in the eastern EC (Wigger et al., 1994; Kley et al., 1996; Schmitz and Kley, 1997). Although crystalline basement is not observed along the mapped transect, the crystalline composition of the concealed basement thrust sheet is justified by (1) the history of early Paleozoic extension and basin formation along the axis of the eastern EC that resulted in eastward tapering and erosion of the Cambrian–Ordovician section and likely deposition of Silurian rocks disconformably on crystalline basement in the IAZ and possibly the SAZ (Kley et al., 1996; Egenhoff, 2007); and (2) Precambrian metagranodiorite exposed at the EC-IAZ boundary at 22°S (Servicio Geologico de Bolivia, 1992; Kley, 1996), 75 km south of our transect, that is involved in thrusting in the eastern EC in northern Argentina (Mingramm et al., 1979; Allmendinger et al., 1983; Mon and Hongn, 1991).

On our cross section, the basement thrust sheet interpreted below the IAZ is drafted as a single intact sheet (e.g., McQuarrie, 2002) that feeds slip forward into the basal Silurian décollement under the SAZ. This geometry requires a corresponding footwall ramp through basement rocks, the location of which is dictated by the total shortening accommodated in the SAZ and Chaco plain. The cumulative slip documented in the SAZ and Chaco plain (Plate 2) restores the eastern edge of the basement thrust sheet to the subsurface projection of the eastern limb of the Camargo syncline, a regional-scale fold in the eastern part of the EC (Plate 2). The 35°–40° west-dipping rocks in the eastern limb of the Camargo syncline are therefore interpreted to reflect the subsurface geometry of a basement footwall ramp. This interpretation is validated by seismic reflection data at ~75 km along strike to the south that reveal an interpreted 35°–40° west-dipping ramp at the same across-strike location and depth below the Camargo syncline as our basement footwall ramp (Plate 2, annotation 12; Allmendinger and Zapata, 2000). The thickness of the interpreted basement thrust sheet is equal to the increase in structural elevation across the SAZ-IAZ transition (~11 km), and the geometry of the leading edge corresponds to the footwall cutoff angle imaged below the Camargo syncline (~35°–40°) (Plate 2).

Our IAZ geometry differs from published cross sections along this transect, which have characterized the subsurface geometry of the cover sequence as dominated by east-vergent thrust faults and folds, and have interpreted the geometry of the leading edge of the basement thrust sheet as an imbricate fan rather than a single intact sheet (Kley, 1996; Kley et al., 1996; Müller et al., 2002; Elger et al., 2005; Oncken et al., 2006). Both interpreted basement geometries are plausible, as the surface geometry data do not favor one model over the other, and no basement rocks are exposed at the IAZ-SAZ boundary. However, the imbricated basement sheet model implies a different footwall ramp position (further east) than the single intact thrust sheet model, and requires a footwall geometry characterized by a series of ramps that progressively step up through ~11 km of basement rock over an east-west distance of ~75 km (e.g., Kley, 1996), rather than a flat décollement underlying the basement thrust sheet. In addition, our interpreted subsurface geometry is consistent with the height, dip, and across-strike location of the footwall ramp imaged in seismic data ~75 km to the south (e.g., Allmendinger and Zapata, 2000) and the subhorizontal velocity discontinuity that extends from the Chaco plain to the top of this footwall ramp (Wigger et al., 1994; Schmitz and Kley, 1997). Furthermore, our interpreted intact basement sheet geometry is mechanically favorable because the weak basal Silurian shale, which is interpreted as a regional décollement level (e.g., Baby et al., 1992; Dunn et al., 1995), is continuously

exploited as slip transitions from the IAZ to the SAZ, instead of breaking new, steeply dipping faults through stronger crystalline basement. This geometry also allows us to more clearly define the IAZ-SAZ boundary as the eastern tip of the basement thrust sheet, and the IAZ-EC boundary at the westernmost backthrust just north of the town of Tarija (Plates 1 and 2).

The timing of Andean deformation within the IAZ is broadly bracketed between ca. 25 and 10 Ma (Gubbels et al., 1993; Horton, 2005; Ege et al., 2007), but the sequence and rate at which the deformation progressed are unknown. Therefore, deformation in the IAZ is assumed to have progressed in sequence from west to east.

Eastern Cordillera

The EC is bound on the east by the Sama-Yunchara anticlinorium, and on the west by the west-vergent San Vincente thrust (Plates 1 and 2). The EC is structurally elevated with respect to the Altiplano and IAZ, and the change in exposure level from the IAZ (mainly Devonian–Silurian rocks) to the EC (lower Ordovician–Cambrian rocks) requires that the primary décollement horizon is located within a deeper stratigraphic level than in the IAZ and SAZ. Basement-involved deformation is required to explain the structural elevation of the EC because the basal décollement of the SAZ-IAZ projects below the deepest Paleozoic sedimentary rocks in the EC and Altiplano (Plate 2; e.g., McQuarrie, 2002; McQuarrie et al., 2008b). Furthermore, seismic refraction and gravity data across the EC preclude imbrication or doubling of the Paleozoic sedimentary section to fill this space (Götze et al., 1994; Wigger et al., 1994; Kley et al., 1996).

The interpreted basement geometry in the EC is important because it influences how deformation at depth balances shortening observed at the surface, and the kinematic style through all levels of the thrust belt (e.g., cf. Plate 2 in this paper and fig. 12 of Müller et al., 2002). Two end-member geometries for basement deformation of the EC have emerged: (1) an east-vergent stack of long, thick basement thrust sheets that feed slip into a principal décollement located at the basement-cover interface via a roof thrust system (e.g., McQuarrie, 2002; McQuarrie et al., 2005, 2008b; Eichelberger et al., 2013), or (2) basement rocks that are deformed through duplexing, or by multiple, deep-seated east- and west-vergent basement faults that both feed slip into and cut across the sedimentary cover interface (e.g., Baby et al., 1997; Müller et al., 2002; Elger et al., 2005; Oncken et al., 2006).

The geophysically imaged crustal structure across the EC at 21°S is characterized by subhorizontally oriented velocity domains, with an interpreted basement-cover interface located at a relatively shallow depth of ~7–10 km below sea level (Plate 2, annotation 17; Wigger et al., 1994; Schmitz and Kley, 1997). In addition, a subhorizontal band of strong mid-crustal reflections seismically imaged at ~7–13 km below sea level under the Camargo syncline at 22°S is interpreted as the basal EC décollement (Plate 2, annotation 12; Allmendinger and Zapata, 2000). The subsurface projection of the basement-cover interface below the Camargo syncline matches with the depth and geometry of horizontal mid-crustal reflections imaged ~75 km to the south (Allmendinger and Zapata, 2000) as well as the ~8–10 km depth to the velocity discontinuity across the central and western EC at ~21°S (Wigger et al., 1994). We therefore interpret the main décollement horizon for upper crustal shortening to be relatively flat, and located at the basement-cover interface (e.g., McQuarrie, 2002; McQuarrie et al., 2008b; Eichelberger et al., 2013). At deeper levels, teleseismic data show subhorizontal low-velocity zones at ~15–20 km depth across the western EC, and at ~30 km depth across the central EC at ~20°S (Beck and Zandt, 2002). The depth to these mid-crustal low-velocity zones is consistent with the depth to décollement for a stack of two ~10–12-km-thick basement thrust sheets (Plate 2; McQuarrie et al., 2005). Interpretation of multiple east- and west-vergent basement faults or duplexing of basement would impart a complex structural topography that is not observed in the EC, and is not demonstrably kinematically viable (McQuarrie, 2002; McQuarrie et al., 2008b). Also, flexural modeling suggests that deep-seated basement faults in the EC would have produced excessive subsidence and much thicker synorogenic sedimentary thicknesses than are observed in the Chaco plain (Prezzi et al., 2009).

The stacked basement thrust sheet model, with an upper crustal décollement located at the basement-cover interface, is therefore favored in this reconstruction because it is most compatible with the observed features discussed here. It is also the simplest kinematic approach to balancing basement and upper crustal shortening, with a geometry that accounts for the structural steps across the tectonomorphic zones (McQuarrie et al., 2008b). Such a basement geometry has long been argued for the central Andes (McQuarrie and DeCelles, 2001; McQuarrie, 2002; McQuarrie et al., 2005, 2008b; Horton, 2005; Eichelberger et al., 2013), and similar basement megathrust sheets are documented in other orogens (e.g., Mitra, 1978; Boyer and Elliott, 1982; Hatcher and Hooper, 1992; DeCelles and Mitra, 1995). Furthermore, numerical models show that orogens loaded by moderate to thick syntectonic sedimentary deposits can develop long, thick, crustal-scale basement thrust sheets (Erdos et al., 2015). However, the present-day average crustal velocities observed for the Altiplano and the presence of localized partial melts at ~14–20 km depths at the Altiplano-EC transition (Beck and Zandt, 2002) are unlikely to sustain the development of the discrete basement faults that we interpret at the western edge of our cross section. Instead, we acknowledge that deformation at these depths may be more diffuse, perhaps occurring along shear zones of as much as kilometer-scale thickness.

Based on the dominant vergence direction of structures, the EC is further divided into two zones (e.g., McQuarrie and DeCelles, 2001; McQuarrie, 2002), discussed in the following.

Eastern Forethrust Zone

The eastern forethrust zone encompasses the region from the IAZ-EC boundary to the Nazareno basin (Plate 1), and is characterized by two regional-scale structures: the Sama-Yunchara anticlinorium and the Camargo syncline (Plate 1). The ~55-km-wide, north-plunging Sama-Yunchara anticlinorium (Kley, 1996) is a structural high observed continuously along the eastern mar-

gin of the EC from northern Argentina to northern Bolivia (Allmendinger and Zapata, 2000; McQuarrie, 2002). The eastern limb consists of an ~10°–20° east-dipping homocline of an ~12-km-thick, structurally intact section of Ordovician to Devonian rocks (Plates 1 and 2). The western limb dips ~5°–40° west toward the hinge zone of the Camargo syncline, where lower Ordovician rocks are unconformably overlain by Cretaceous rocks (Plate 1). North-trending, ~3–7-km-wavelength fault-propagation folds are superimposed on the broader anticlinorium, and grew above low-offset (~1–3 km), generally east-vergent thrust faults (Plate 2).

The western limb of the anticlinorium is interpreted as a ramp anticline above a deep-seated basement footwall ramp, and the eastern limb corresponds to a hanging-wall ramp that must cut upsection to the east from basement through the Cambrian–Ordovician section (Kley, 1996; Kley et al., 1996). Deformation in the EC and IAZ is linked to progressive eastward emplacement of the same basement thrust sheet, which is stacked above the basement thrust sheet that feeds slip into the SAZ. However, we interpret the structurally higher basement thrust sheet as a tectonic wedge that distributes a component of its slip into the sedimentary cover sequence in the EC via a west-vergent roof thrust system at the basement-cover interface (e.g., McQuarrie, 2002; Horton, 2005) and the remainder of its slip forward into the sedimentary cover of the IAZ (Plate 2). This model allows the simplest basement geometry interpretation because it requires only one major basement footwall ramp for EC-IAZ deformation (Plate 2).

The Camargo syncline is traceable for ~780 km from northern Argentina to central Bolivia. On our transect, the syncline exhibits a gently dipping eastern limb and a steeply dipping to overturned western limb. The western limb is bound by an east-vergent thrust fault that places Ordovician rocks over Mesozoic–Paleocene rocks. The difference in metamorphic grade of Ordovician rocks on either side of the syncline suggests pre-Cretaceous vertical offset (Müller et al., 2002; Jacobshagen et al., 2002). Where the depositional contact is exposed, Cretaceous rocks in the western limb overlie Ordovician rocks that are ~3 km stratigraphically deeper than on the eastern limb (Servicio Geologico de Bolivia, 1992; Plate 1). However, the overlying Paleogene rocks are folded into a tight anticline inset within the larger syncline (Plate 2, annotation 14). Therefore, we interpret a west-dipping, pre-Andean thrust fault below the Camargo syncline that was reactivated during Andean deformation.

Between the Camargo syncline and the Nazareno basin (Plate 1), lower Ordovician rocks are deformed by tight folds (~1–2 km wavelength) and closely spaced (~1–2 km) thrust faults with stratigraphic separations typically ≤2 km (Plate 2). This interpretation is in contrast with that of Müller et al. (2002), who interpreted the region between the Camargo syncline and Nazareno basin as a west-vergent imbricate fan.

Western Backthrust Zone

The western backthrust belt of the EC has long been recognized as a continuous along-strike feature throughout much of the central Andes (Kley et al., 1997; Baby et al., 1997; McQuarrie and DeCelles, 2001; Müller et al., 2002). However, differing structural interpretations in the Tupiza region (Horton, 2000; Sempere, 2000) have hindered efforts to obtain reliable shortening estimates through a significant portion of the western EC along our transect (Müller et al., 2002). Through reexamination of key structural and stratigraphic relationships (Figs. SM1–SM5; see footnote 1), and construction of a sequentially restored section (Fig. SM6) that matches the synorogenic depositional history of the Cenozoic sedimentary basins near Tupiza (e.g., Hérail et al., 1996; Horton, 1998; Sempere, 2000; Müller et al., 2002), we show that thrust faults and folds are dominantly west vergent from the western edge of the Nazareno basin to the easternmost Altiplano (Plates 1 and 2). This interpretation facilitates a balanced solution through the Tupiza region that kinematically links deformation between the eastern and western halves of the EC, and allows us to quantify the magnitude of out-of-sequence shortening that was previously unconstrained. A detailed discussion of the sequential restoration through the Tupiza region is included in Supplementary Material sections 2 and 3 (see footnote 1).

The eastern half of the backthrust belt (Nazareno basin to Estarca basin) is characterized by five Cenozoic basins bound on at least one of their margins by thin, west-vergent thrust sheets (~1–2 km) carrying middle-upper Ordovician rocks. The structural grain is north-trending (350°–010°), faults are closely spaced (~1–4 km) with maximum displacements of ~2–4 km, and folds are short wavelength (<2 km). The western half of the backthrust belt was constructed as an imbricate thrust system that soles into a higher, secondary décollement at the base of the middle Ordovician section (Plate 2). Thrusts carrying thick, east-dipping sheets of upper Ordovician rocks are widely spaced (~5–12 km), with maximum displacements of ~5–10 km. West of the Estarca basin, thrust faults and folds trend 345°–350°. This oblique structural grain is only observed in Ordovician rocks and may be attributed to a pre-Andean structural fabric that was reactivated during Andean deformation (Müller et al., 2002).

We include the easternmost Altiplano in our description of the EC, as these two zones are kinematically linked (Elger et al., 2005). In the footwall of the San Vincente thrust, well logs and seismic data reveal ~2–3 km of Cenozoic synorogenic rocks above ~11 km of Paleozoic–Mesozoic sedimentary rocks (Welsink et al., 1995; Elger et al., 2005). This constrains the depth to basement in the eastern Altiplano at ~13 km below sea level and reveals ~6 km of vertical offset of the basement-cover interface across the Altiplano-EC boundary (Plate 2, annotation 22). This structural step has been attributed to a west-dipping monocline of basement rock (Müller et al., 2002; Elger et al., 2005). However, because the EC is modeled here as a roof thrust system above a basement thrust sheet, we interpret this structural step as the basement footwall ramp that corresponds to the hanging-wall ramp described at the IAZ-EC boundary (e.g., McQuarrie and DeCelles, 2001; McQuarrie, 2002). West of the San Vincente thrust (Plate 1 and Plate 2, annotation 23), mapping (Servicio Nacional de Geologica y Tecnico de Minas, 2010) and seismic reflection data (Elger et al., 2005) define a broad wavelength (>20 km) anticlinorium of Paleozoic rocks with secondary, shorter wavelength (~10 km) folds in overlying Cenozoic synorogenic rocks. A third, westernmost basement thrust sheet (Plates 1 and 2, western basement sheet)

is interpreted to structurally elevate Paleozoic rocks by passing over a footwall ramp and feeding slip into the basement-cover interface below the EC and easternmost Altiplano (e.g., McQuarrie, 2002, Fig. 3 therein).

Restoring the EC to the upper Cretaceous horizontal datum reveals the presence of the probable Jurassic Tupiza rift basin (e.g., Sempere, 1994; Sempere et al., 2002), and a pre-Mesozoic (likely late Paleozoic) west-dipping monocline (e.g., Müller et al., 2002) (Plate 2, annotation 22). Cenozoic AFT ages support a locally thick Mesozoic section near Tupiza (Ege et al., 2007), but we show that extension and later inversion of normal faults was likely low magnitude (Plate 2, annotation 19; Fig. SM6 [see footnote 1]). A pre-Cretaceous (likely Carboniferous) crustal shortening event has also been interpreted in the EC; however, this event produced subvertical penetrative cleavage and small-scale folding in Ordovician rocks rather than a system of discrete, large-offset faults (Kley et al., 1997; Jacobshagen et al., 2002; Müller et al., 2002). Except where pre-Andean offsets are noted, all shortening in our estimate is related to Andean deformation.

AFT ages are interpreted to mark the onset of deformation in the central EC ca. 40–36 Ma, which spread toward the Altiplano and IAZ from ca. 33 to 25 Ma (Ege et al., 2007). Later phases of deformation in the EC are typically not well resolved (Ege et al., 2007), but the sequential restoration through the western Cenozoic outcrop belt (Fig. SM6 [see footnote 1]) reveals 20 km of west-vergent, out-of-sequence deformation between ca. 29 and 10 Ma, contemporary with eastward advance of the deformation front through the IAZ (Horton, 2005; Ege et al., 2007).

CRUSTAL SHORTENING ESTIMATES

Crustal shortening is calculated from the measured difference between the line length-balanced deformed and undeformed cross sections in Plate 2 (results summarized in Table 1). Uncertainty in the shortening estimate is assessed by producing an area-balanced solution, which permits formal propagation of errors on input parameters such as stratigraphic thickness, depth to décollement, and eroded hanging-wall cutoffs (e.g., Judge and Allmendinger, 2011; Allmendinger and Judge, 2013) (detailed discussion in Supplementary Material [see footnote 1]). The line-length balanced and area-balanced solutions for total shortening produce similar results, both for the thrust belt as a whole and for individual tectonomorphic zones (Table 1; Tables SM1 and SM2 [see footnote 1]). Error magnitudes are reported assuming a Gaussian distribution of uncertainty (Judge and Allmendinger, 2011).

Shortening estimates for each tectonomorphic zone are shown in Table 1. The EC accommodated 120 km of shortening (37%), and the IAZ accommodated 70 km (70%). Individual estimates of uncertainty for the EC and IAZ were not possible due to the limitations of the area balance software for the complex deformation geometry at the IAZ-EC boundary (e.g., Judge and Allmendinger, 2011; Supplementary Material [see footnote 1]). However, we combined the two zones because they are kinematically linked, resulting in a shortening estimate of 190 ± 46 km (43% ± 6.9%). The SAZ accommodated 82 ± 21 km of shortening (36% ± 6%). The total shortening estimate from the EC, IAZ, and SAZ is 272 ± 67 km (42% ± 7.8%). The total retroarc shortening was determined by adding our estimate to the 65 km of shortening estimated for the Altiplano at this latitude (Elger et al., 2005), for a total of 337 ± 69 km of shortening (36% ± 7%).

Previous total shortening estimates at 21°S are based on a composite of cross sections through individual tectonomorphic zones (Table 2), and vary depending on the combination of structural studies used, from a minimum of 199 km (Dunn et al., 1995; Kley, 1996; Müller et al., 2002; Elger et al., 2005) to a maximum of 319 km (Kley, 1996; Baby et al., 1997; Müller et al., 2002). The maximum composite shortening estimate is within our uncertainty range, but our range is above the 199 km minimum. Although our estimate of SAZ shortening is ~20 km less than the previous estimates at this latitude (Tables 1 and 2), it is comparable to other SAZ shortening estimates between 15° and 23 °S (60–86 km; Table 3). The overall increase in total shortening arises from our deformation geometries in the IAZ and EC that differ from published cross sections, and by accounting for the unbalanced Tupiza segment in the EC.

Given the significant errors that we estimate for individual tectonomorphic zones, it is important to place these uncertainties in context (e.g., Eichelberger et al., 2013). The area-balance solution is not constrained by any particular

TABLE 1. CROSS-SECTION SHORTENING ESTIMATES AT 21°S

	Original length (km)	Final length (km)	Total shortening (km)	Total shortening (%)
Subandean zone (SAZ)	226	144	82 ± 21	36 ± 6
Interandean zone (IAZ)	100	30	70	70
Eastern Cordillera (EC)	324	204	120	37
(EC and IAZ combined)	424	234	(190 ± 46)	(43 ± 6.9)
Total (EC to SAZ)	650	378	272 ± 67	42 ± 7.8
Altiplano*	279	214	65	23
Total (entire backarc)†	929	592	337 ± 69	36 ± 7

*Shortening estimate from Elger et al. (2005).
†Entire backarc estimate is calculated by combining our estimate of shortening for the EC to SAZ with the shortening estimate for the central and western Altiplano (Elger et al., 2005).

TABLE 2. PUBLISHED CROSS-SECTION SHORTENING ESTIMATES AT 21°S

	Subandean zone (km)	Interandean zone (km)	Eastern Cordillera (km)	Altiplano (km)
Dunn et al. (1995)	100	59		
Kley (1996)	99	45		
Kley et al. (1997)			55–80	
Baby et al. (1997)			88	20
Müller et al. (2002)			35–95	
Elger et al. (2005)				65
Minimum shortening estimate (km)		199		
Maximum shortening estimate (km)		319		

Note: Maximum and minimum shortening estimates are a composite from multiple studies rather than a single continuous cross-section line.

kinematic model, and provides a shortening estimate that encompasses all line-length balance solutions for a given area (Judge and Allmendinger, 2011). In contrast, the line-length balanced cross section (Plate 2) considers geometric constraints from geophysical and map observations, and is balanced by slip on the underlying basement thrust sheets (e.g., viability; Woodward et al., 1989). As a consequence, increasing or decreasing the magnitude of shortening will result in a change in footwall and hanging-wall cutoff positions. Given the known thicknesses of the Paleozoic–Mesozoic section from geologic mapping, the location of the Camargo syncline, and the geophysical constraints on the positions of the footwall and hanging-wall cutoffs of the SAZ basement thrust sheet (Plate 2, annotations 6a and 12), errors as large as ±20 km in the SAZ are difficult to reconcile. However, given the lack of constraints on the basement geometry below the EC (Plate 2, annotations 6a and 22), it is possible to allow for a ±46 km (or even ±69 km) change in the position of the EC-IAZ basement sheet footwall ramp, or a different basement geometry altogether (e.g., Baby et al., 1997; Müller et al., 2002). We state this with the caveat that any change to the basement geometry must still honor the consistent structural level observed across the EC and the changes in structural elevation at the EC-IAZ and EC-Altiplano boundaries.

At a broader scale, the shortening estimate must also be compatible with the regional kinematics required for the development of the Andean oroclinal bend. Our central estimate of total shortening is comparable with the patterns of retroarc shortening estimated from balanced cross sections throughout the central Andes (Fig. 3). The highest shortening magnitudes occur near the central core of the orocline (17°–21°S), but decease substantially along strike to the north and south. Given this along-strike shortening gradient, our shortening estimate range (268–406 km) should produce clockwise rotations of ~5°–15° in the southern limb of the orocline (e.g., Kley, 1999). This is consistent with ~6°–14° limb rotations predicted from simplified reconstructions of the orocline and observed paleomagnetic rotations (Eichelberger et al., 2013; Eichelberger and McQuarrie, 2015). Although the upper end of our estimate is rather large, it is still compatible with (but at the limit of) the crustal shortening predicted by regional models of oroclinal bending (Fig. 3; Arriagada et al., 2008). However, more robust three-dimensional (3D) kinematic models that consider the complex map-view kinematics that occur during development of curvature in the core of the central Andean orocline predict ~320–350 km of shortening in the southern limb (Fig. 3; Eichelberger and McQuarrie, 2015), on par with our shortening estimate of 337 km.

TABLE 3. ALONG-STRIKE ESTIMATES OF SHORTENING IN THE CENTRAL ANDES

Latitude (°S)	Altiplano-Puna (km)	Eastern Cordillera (km)	Interandean zone (km)	Subandean zone (km)	Total (km)
12–14[a]	15	91		17	123
13–15[b]		99		31	130
15–17[c]		123	48	66	237
17–18[d]	47	142	39	72	300
19[e]	48	136	43	86	313
20[d]	41	122	96	67	326
21[f,g]	65	**120**	**70**	**82**	**337**
22–23[h,i,j]	50	95		60	205
24–25[k,l,m]	26	95		21	142

Note: Compilation of along-strike shortening estimates of the central Andes from balanced cross sections. Estimates in this study are in bold. Superscript denotes source: a—Gotberg et al. (2009); b—Perez et al. (2016); c—McQuarrie et al. (2008); d—McQuarrie (2002); e—Eichelberger et al. (2013); f—this study; g—Elger et al. (2005); h—Echavarria et al. (2003); i—Kley and Monaldi (1999); j—Cladouhos et al. (1994); k—Pearson et al. (2013); l—Kley and Monaldi (2002); m—Coutand et al. (2001).

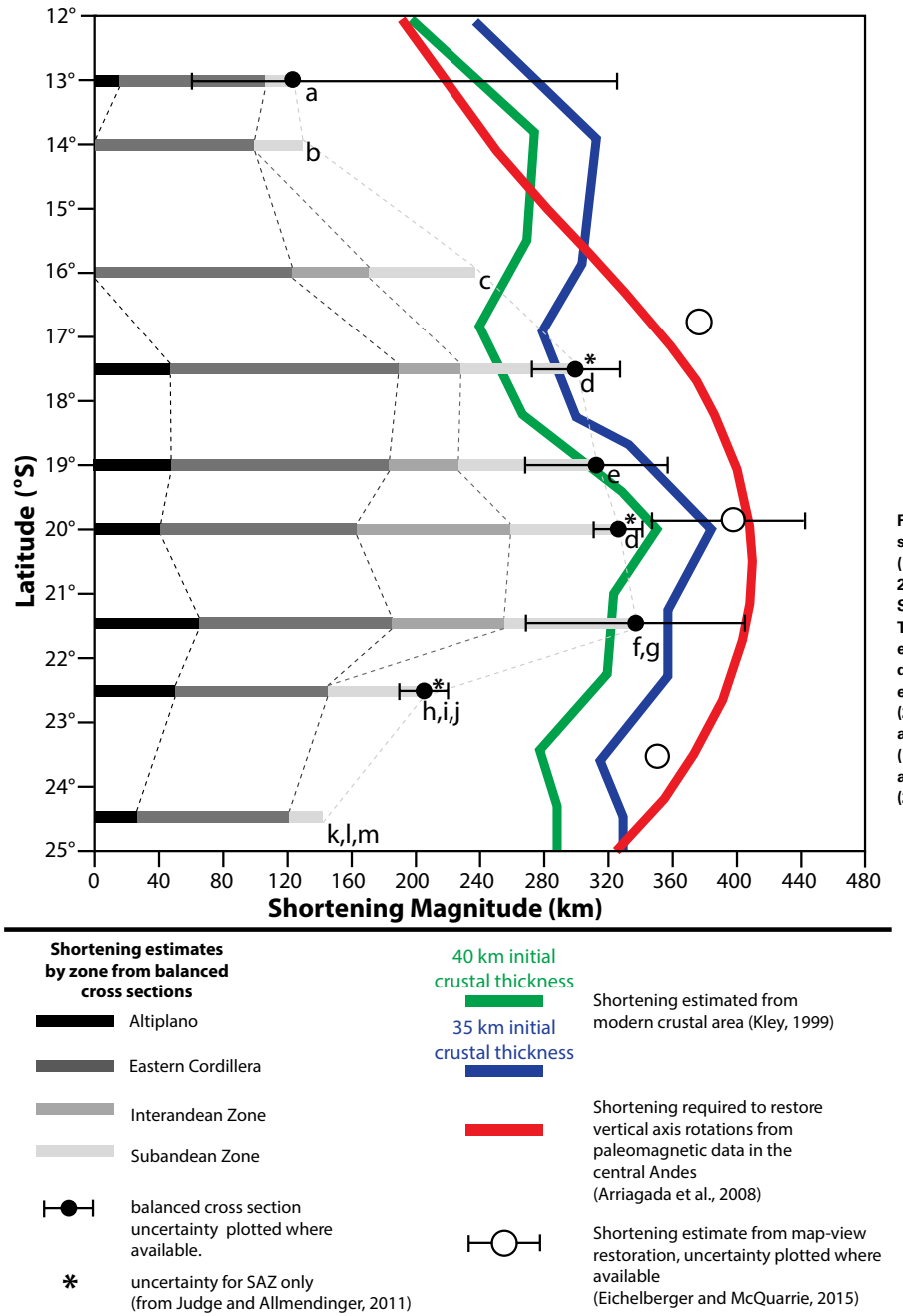

Figure 3. Along-strike comparison of shortening estimates in the central Andes (13°–25°S) (modified from Gotberg et al., 2010; Eichelberger and McQuarrie, 2015). Sources of shortening estimates (also see Table 3): a—Gotberg et al. (2010); b—Perez et al. (2016); c—McQuarrie et al. (2008b); d—McQuarrie (2002); e—Eichelberger et al. (2013); f—this study; g—Elger et al. (2005); h—Echavarria et al. (2003); i—Kley and Monaldi (1998); j—Cladouhos et al. (1994); k—Pearson et al. (2013); l—Kley and Monaldi (2002); m—Coutand et al. (2001). SAZ—Subandean zone.

For these reasons, we consider our central estimate to be the most reliable estimate, because it is derived from a kinematically consistent reconstruction, and also closely matches the crustal shortening predicted from the 3D kinematic model of the central Andean orocline. However, the minimum and maximum shortening estimates cannot be totally discounted, because looser constraints on the EC and Altiplano basement geometry allow for the freedom to modify the crustal ramp locations without violating regional kinematic constraints.

DISCUSSION

Kinematic Development of the Retroarc Fold-Thrust Belt

Our cross section provides a new geometric and kinematic model for the development of the retroarc thrust belt at 21°S that is compatible with published cooling ages (Ege et al., 2007) and the foreland basin migration history (Gubbels et al., 1993; Horton, 1998, 2005; Echavarria et al., 2003; Uba et al., 2009) in southern Bolivia (Fig. 4), and is consistent with recent models of the Andean thrust belt in central and northern Bolivia (McQuarrie, 2002; McQuarrie et al., 2005, 2008b; Horton, 2005; Eichelberger et al., 2013). The majority of deformation in the EC and IAZ is linked to earlier emplacement of the upper basement thrust sheet (Figs. 4B–4D), with a separate, westernmost basement thrust sheet that fed a minor amount of slip (~30 km) into the EC and easternmost Altiplano (Fig. 4C). Deformation in the SAZ is linked to emplacement of the younger, lowermost basement thrust sheet (Fig. 4E).

Although climatic effects such as orographic precipitation may exert a control on the distribution of cooling ages, especially in the northern Bolivian Andes (Barnes et al., 2012), the timing of deformation and initial rapid exhumation are synchronous in the central Andes (Barnes and Ehlers, 2009). In particular, AFT ages demarcating initial cooling are related to uplift and exhumation accompanying eastward propagation and passage of basement thrust sheets over large-scale footwall ramps (Barnes et al., 2008; McQuarrie et al., 2008b). In our cross section, the footwall ramp of the upper basement thrust sheet is restored to a position directly below the central EC (Fig. 4A), where ca. 40–36 Ma AFT ages (Ege et al., 2007) are interpreted to mark the initiation of deformation and uplift as the basement sheet began propagating eastward (Fig. 4B). AFT ages of ca. 33–25 Ma define the westward and eastward expansion of deformation into the backthrust and forethrust belts of the EC (Ege et al., 2007), contemporary with deposition and eastward migration of foredeep deposits (Fig. 4C; DeCelles and Horton, 2003; Horton, 2005). This bivergent expansion of exhumation is explained by insertion of the upper basement sheet as a tectonic wedge, because vertical uplift should occur both above the active basement footwall ramp and above the advancing tip of the basement sheet as it was wedged eastward (Fig. 4C). As deformation was distributed into the sedimentary cover in both the EC backthrust and forethrust belts via a west-directed roof thrust system, the upper basement thrust sheet was progressively wedged eastward, which drove flexural subsidence and eastward migration of the foredeep (Fig. 5C). The transition from foredeep to intermontane sedimentation in the EC after ca. 25 Ma, combined with a ca. 18–15 Ma AFT age in the IAZ (Ege et al., 2007), indicates diminished shortening within the EC and eastward migration of the deformation front into the IAZ. The deformation front migrated eastward across the IAZ from ca. 25 to 10 Ma by imbrication of the sedimentary cover in front of the advancing upper basement sheet (Fig. 4D). The kinematics of basement deformation shifted from tectonic wedging to translation of basement slip forward into the décollement below the IAZ (Figs. 4C–4D), possibly as a consequence of thickness changes of Paleozoic rocks across the IAZ-EC boundary, or as weaker Silurian shale at the basement-cover interface was encountered at the western edge of the IAZ. Backthrusting in the western half of the IAZ may have acted as a taper building mechanism in response to a subcritical wedge state, which could have been induced by erosional removal of material from the wedge (Davis et al., 1983; Willett, 1999; Malavieille, 2010), negative isostatic buoyancy from a dense lithospheric root (Kay and Kay, 1993; DeCelles et al., 2009, 2015; Wells et al., 2012), or a change in basin taper due to sedimentary thickness changes between the EC and IAZ (e.g., Boyer, 1995).

Although the majority of shortening between ca. 25 and 10 Ma took place in the IAZ, the west-directed roof thrust system below the EC remained active, at least intermittently, because we estimate >20 km of west-directed, out-of-sequence shortening in the Tupiza region between ca. 25 and 10 Ma (Fig. 4D). The development of the ca. 10 Ma San Juan del Oro erosion surface marks the cessation of deformation in the EC and eastward migration of the deformation front into the SAZ, suggesting that emplacement of the upper basement sheet was complete by this time (Gubbels et al., 1993; Horton, 1998, 2005). A dramatic increase in sedimentation rates of synorogenic rocks in the eastern SAZ beginning ca. 12.4–8.5 Ma, interpreted as the result of enhanced crustal flexure induced by initiation of the lower basement sheet, is inferred as the timing of onset for SAZ deformation (Echavarria et al., 2003; Uba et al., 2009). The deformation front migrated eastward across the SAZ as the sedimentary cover sequence was imbricated in front of the advancing lower basement sheet (Fig. 4E). During this time, the advancing basement thrust sheet drove the flexural foredeep eastward to its current position (Horton and DeCelles, 1997; Prezzi et al., 2009; Uba et al., 2009) while passively translating rocks in the EC and IAZ eastward.

Implications for the Andean Crustal Thickening Budget

Although magmatic addition may be an important mechanism for crustal thickening in Cordilleran orogens (e.g., Allmendinger et al., 1997), numerous studies have demonstrated that horizontal shortening is the most significant contributor to crustal thickening and resultant surface uplift in the central Andes (Isacks, 1988; Sheffels, 1990; Schmitz, 1994; Allmendinger et al., 1997; Baby et al., 1997; Kley and Monaldi, 1998; Kley et al., 1999; McQuarrie and DeCelles, 2001;

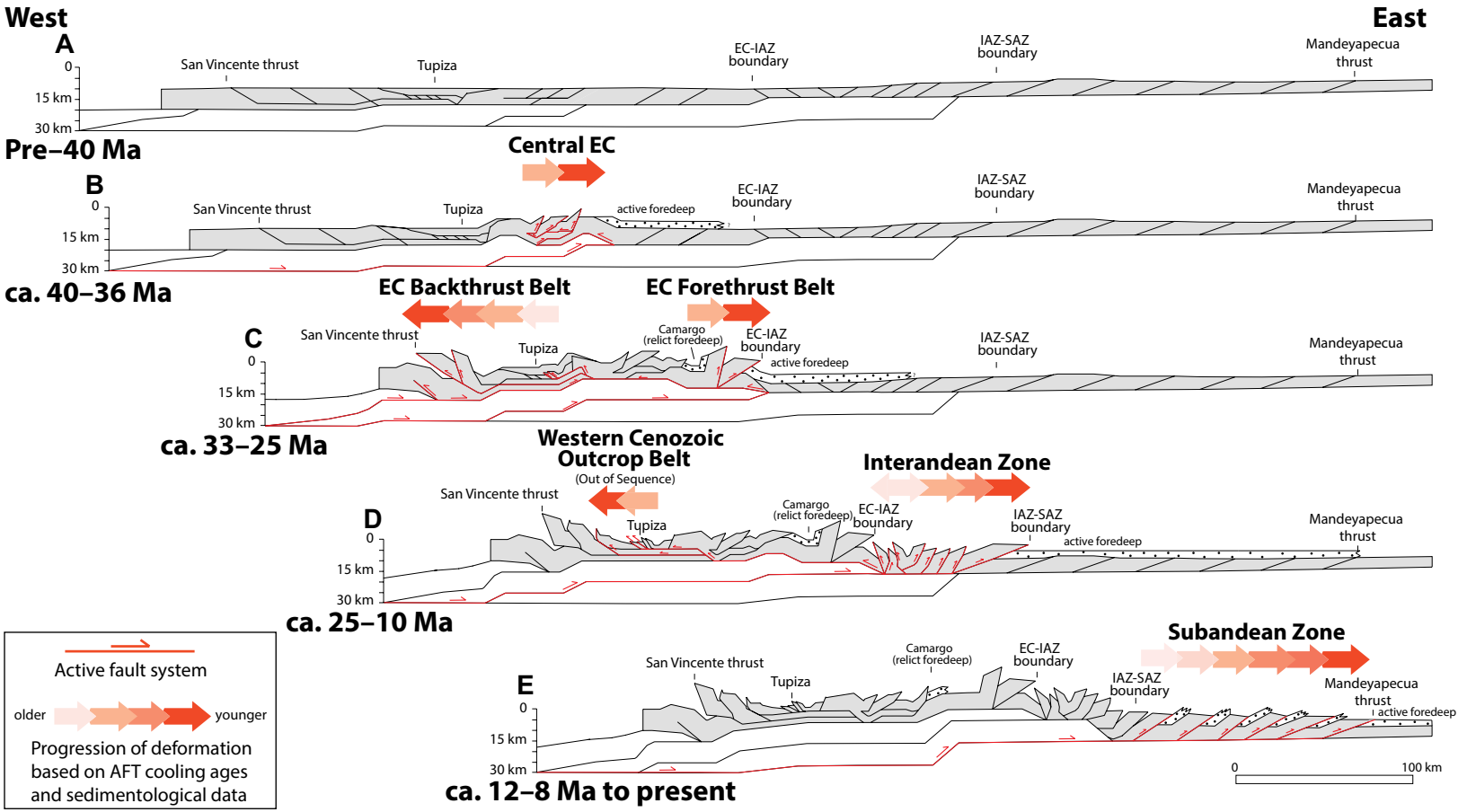

Figure 4. General kinematic model for development of the central Andean retroarc thrust belt at 21°S; structure generalized from Plate 2. Gray shaded area represents pre-Cenozoic sedimentary rocks; white area represents basement rocks; stippled area schematically represents synorogenic foreland basin deposits. Thrust faults active in specific increments are highlighted in red. Timing constraints are from Horton (1998, 2005), Ege et al. (2007), and Uba et al. (2009). AFT—apatite fission track. (A) Pre–40 Ma crustal architecture of the Eastern Cordillera (EC), Interandean zone (IAZ), and Subandean zone (SAZ). (B) From ca. 40 to 36 Ma: activation of upper basement thrust sheet and initiation of exhumation in central EC cover sequence via roof thrusting. (C) From ca. 33 to 25 Ma: continued eastward advance and tectonic wedging of the lower basement sheet concurrent with westward and eastward expansion of deformation and exhumation in the EC cover sequence across the backthrust and forethrust belts. (D) Deformation front migrates eastward through the IAZ from ca. 25 to 10 Ma in front of the upper basement sheet as west-vergent, out-of-sequence deformation occurs in the western Cenozoic outcrop belt via roof thrusting. (E) Cessation of motion on the upper basement thrust sheet and imbrication of the SAZ cover sequence in front of the lower basement thrust sheet from 12–8 Ma to the present.

McQuarrie, 2002; McQuarrie et al., 2005). The crust of a retroarc fold-thrust belt is tectonically thickened as foreland lithosphere is subducted toward the hinterland by an amount equal to the magnitude of upper crustal shortening (Fig. 5A) (DeCelles and DeCelles, 2001). In this basic model, the crustal budget, or the expected cross-sectional area of the crust, is calculated by multiplying the undeformed original length of the thrust belt by an initial preorogenic crustal thickness (Fig. 5A; Kley and Monaldi, 1998; McQuarrie, 2002).

A major uncertainty in the crustal budget calculation is the initial thickness of South American continental crust prior to Cenozoic shortening, which may have varied across strike (McQuarrie, 2002). The undeformed foreland lithosphere at ~21°–20°S has an observed thickness of 35–40 km from teleseismic data (Wigger et al., 1994; Beck et al., 1996; Beck and Zandt, 2002; Baumont et al., 2002). Although Late Triassic to Middle Jurassic (Sempere et al., 2002) and Late Cretaceous (Salfity and Marquillas, 1994) rifting affected southern Bolivia

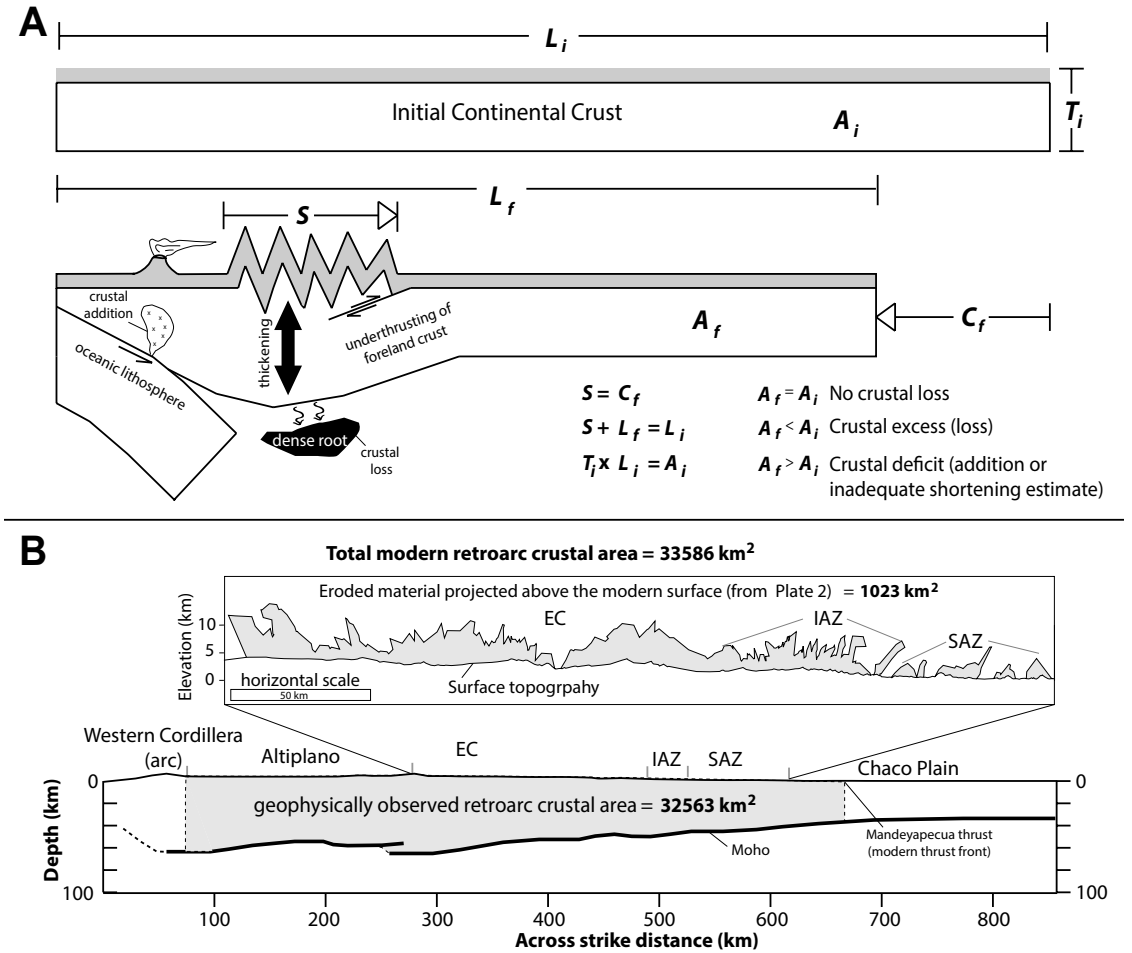

Figure 5. (A) Schematic cross section of an undeformed (upper) and deformed (lower) contractional orogen illustrating the parameters used to calculate the crustal thickness budget of a mountain belt (modified from DeCelles and DeCelles, 2001; DeCelles et al., 2009). Gray shaded area represents the upper crust; white area represents lower crust. L_i—initial length, L_f—final length, A_i—initial cross-sectional crustal area, A_f—modern (observed) cross-sectional crustal area, T_i—assumed initial crustal thickness, S—upper crustal shortening, C_f—foreland convergence. The orogenic wedge is thickened tectonically as upper crustal shortening is accompanied by an equal magnitude of underthrusting of foreland lower crust and mantle lithosphere toward the hinterland. (B) Observed crustal thickness from teleseismic and regional earthquakes at ~21°–20°S (Beck et al., 1996; Beck and Zandt, 2002); bold black line delineates the interpreted Moho (modified from McQuarrie, 2002). The cross-sectional crustal area used in the thickness budget spans the Altiplano to the eastern thrust front, shown by the gray shaded polygon. Eroded material is determined from calculating the area of preorogenic rocks projected above the modern erosion surface in Plate 2. Budget calculations are summarized in Table 4. EC—Eastern Cordillera; IAZ—Interandean zone; SAZ—Subandean zone.

(McGroder et al., 2015), lower crustal granulite xenoliths from the Salta Rift of northern Argentina (~23°–26°S) suggest that crustal thinning was minimal, and that the crust was at least ~35 km thick ca. 90 Ma (Lucassen et al., 1999). In addition, geochemical proxies for crustal thickness (Sr/Y and La/Yb ratios) suggest that the western edge of the South American crust was ~35–43 km thick at the onset of Andean shortening (ca. 80–70 Ma; Profeta et al., 2015). Expected crustal thicknesses are compared to the modern crustal area (Fig. 5B), which includes the geophysically determined crustal area of the orogen at this latitude (~32,563 km²; e.g., Beck et al., 1996; Beck and Zandt, 2002), as well as the area of rock projected above the erosion surface (1023 km²). Along-strike estimates of the crustal thickness budget for the central Andes are displayed in Figure 3.

For a 35-km-thick initial crust, the expected crustal area for the minimum, central, and maximum shortening estimates for the entire retroarc result in a deficit of 3486 km² (90%), a deficit of 1071 km² (97%), and an excess of 1334 km² (104%) compared to the observed crustal area at 21°S (Table 4). For a 40-km-thick initial crust, our range of shortening estimates predicts 2%–18% of excess crustal area (Table 4). Therefore, our shortening estimate range is in agreement with other studies along strike that show that upper crustal shortening can account for, and in some cases exceed, observed modern crustal thicknesses in the central Andes (McQuarrie and DeCelles, 2001; McQuarrie, 2002; DeCelles and Horton, 2003; Hindle et al., 2005; McQuarrie et al., 2005; Eichelberger et al., 2015).

TABLE 4. CRUSTAL THICKNESS BUDGET OF THE CENTRAL ANDES AT 21°S

	Original length (km)	Expected area (km²)		Present-day area (km²)	Crustal area excess or deficit (km²)	
		35 km initial thickness	40 km initial thickness		35 km initial thickness	40 km initial thickness
Central shortening estimate	929	32515	37160		–1071 (97%)	+3574 (110%)
Minimum shortening estimate	860	30100	34400	33586	–3486 (90%)	+814 (102%)
Maximum shortening estimate	998	34930	39920		+1344 (104%)	+6334 (118%)

Note: Crustal area was calculated from gray shaded area in Figure 6 (see text). Note that the area curves in Figure 4 are for the entire across-strike area of the mountain belt, whereas the area calculated here (and Fig. 6) only encompass the retroarc (i.e., Altiplano to easternmost thrust front).

Excess crustal area implies a loss or redistribution of material, either by lower crustal flow or delamination of dense lower crust (Beck and Zandt, 2002). Accordingly, because the thick crust below the central Andes of southern Bolivia is predominantly felsic, the mafic component of the lower crust is interpreted to be missing (Beck and Zandt, 2002). Delamination of dense eclogitic lower crust and mantle lithosphere has been called upon as a mechanism to explain the absence of a mafic lower crust, as well as a cause for rapid Miocene surface uplift events in the EC and Altiplano (Garzione et al., 2006, 2008, 2014; Molnar and Garzione, 2007). Petrologic and numerical models indicate that crustal thicknesses of ≥50 km are required to generate eclogitic phases from mafic lower crust (Kay and Kay, 1993), and that thicknesses of ≥45–50 km must be achieved to drive lower crustal flow (Husson and Sempere, 2003). Furthermore, numerical models emphasize that a sufficient thickness (~10 km) of eclogitic lower crust must be lost along with the mantle lithosphere in order to significantly affect surface elevation (Garzione et al., 2006; Hoke and Garzione, 2008; Krystopowicz and Currie, 2013; Wang et al., 2015). Therefore, in order to provide insight into the potential geodynamic processes that operated in the Andean retroarc at the latitude of our study area, it is necessary to highlight where crustal thickening was distributed in the retroarc region (e.g., Eichelberger et al., 2015), and when critical thicknesses may have been achieved.

The mode of deformation that accommodates lithospheric thickening (i.e., pure shear versus simple shear), which will affect the distribution of crustal thickening (e.g., Allmendinger and Gubbels, 1996), likely differs across the retroarc in both space and time. The crust beneath the Altiplano and EC in southern Bolivia is weak and isostatically compensated, which favors pure shear deformation (Beck et al., 1996; Beck and Zandt, 2002). In contrast, the IAZ and SAZ are flexurally supported by the rigid Brazilian lithosphere, and therefore likely deform by simple shear (Lyon-Caen et al., 1985; Dorbath et al., 1993; Beck and Zandt, 2002; Eichelberger et al., 2015). We modify our crustal budget calculation (Fig. 5A) to account for differing modes of deformation, similar to the models presented in Isacks (1988, Fig. 4 therein) and Eichelberger et al. (2015, Fig. 5 therein). We assume that horizontal upper crustal shortening in the Altiplano and EC was accompanied by vertical thickening of the underlying lower crust via pure shear. Shortening of the SAZ-IAZ occurs by upper crustal imbrication focused along the eastern margin of the thrust belt, and the rigid lithosphere compresses and thickens the ductile lower crust beneath the Altiplano-EC. Because the locus of thickening occurs below the EC-Altiplano, crustal thicknesses are approximated by dividing the area added during each major shortening increment (e.g., Fig. 5; 40–27 Ma, 25–10 Ma, 10 Ma to present) by the deformed length of the EC-Altiplano. The nominal thickening of the IAZ and SAZ by imbrication of basement thrust sheets is accounted for and not included in the thickening below the EC-Altiplano. Because it is difficult to ascribe the precise location and timing of our shortening errors (±69 km), we assign the shortening uncertainties to the EC and Altiplano, and divide them between the periods ca. 40–27 Ma and ca. 25–10 Ma. Although this model is simplistic, it sets a basic benchmark calculation for the distribution of crustal thickness through time.

Given the general timing constraints (Fig. 4), our range of shortening estimates, and an initial crustal thickness of 35 km, the EC and Altiplano are predicted to have achieved thicknesses of 43 ± 3 km by ca. 27 Ma, 56 ± 5.5 km by 10 Ma, and 64 ± 5 km by the present. Critical thicknesses (>45–50 km) required for phase changes of mafic material to dense eclogite, or for initiation of lower crustal flow, were achieved by 10 Ma. However, because the final estimated crustal thicknesses closely match the modern average thickness (~65 km) observed across the EC and Altiplano (Fig. 5), it is unlikely that significant thicknesses of lower crust were removed.

For an initial crustal thickness of 40 km, the EC and Altiplano are predicted to have achieved thicknesses of 49.5 ± 3.5 km by ca. 27 Ma, 64.5 ± 5.5 km by 10 Ma, and 74 ± 5.5 km by the present. Critical thicknesses in the EC and Altiplano were achieved by ca. 27 Ma, and predicted crustal thicknesses match modern thicknesses (~65 km) by ca. 10 Ma. Predicted thicknesses of 74 ± 5.5 km by the present exceed the observed thicknesses, suggesting that loss of an ~2.5–14.5-km-thick section of lower crust across the EC and Altiplano is possible, which is large enough to have a significant effect on hinterland surface elevation.

CONCLUSIONS

The SAZ, defined by 10–20-km-wavelength, 4–6-km-amplitude fault-bend folds above a 10–12-km-deep regional décollement in Silurian rocks, accommodated 82 km (36%) of east-west shortening. The IAZ, a bivergent zone of 2–4-km-thick thrust sheets of mainly Silurian–Devonian rocks that are struc-

turally elevated ~10 km relative to adjacent SAZ, accommodated 70 km (70%) of shortening. The EC, a bivergent zone of 2–10-km-thick thrust sheets of Cambrian–Ordovician rocks structurally elevated ~6 km relative to both the IAZ and Altiplano, accommodated 120 km (37%) of shortening. Combined with a published estimate of 65 km of shortening for the Altiplano, total shortening of the Andean retroarc thrust belt at 21°S is 337 ± 69 km (36% ± 7%).

Thrust belt development was controlled by emplacement of two long thick basement thrust sheets. The upper basement sheet was tectonically wedged eastward, and fed slip into the sedimentary cover of the overlying EC via a west-vergent roof thrust system from ca. 40 to 25 Ma. The sedimentary cover in the IAZ was deformed in front of the upper basement sheet, which fed slip into a décollement within Silurian shale, from ca. 25 to 10 Ma. Approximately 25 km of out-of-sequence deformation in the western EC, between ca. 29 and 10 Ma, was contemporaneous with eastward migration of the deformation front through the IAZ. The SAZ was deformed in front of a lower basement sheet, which also fed slip into a décollement within Silurian shale, beginning ca. 12–8 Ma. This model is consistent with the patterns of published cooling ages and the record of deposition and eastward migration of the central Andean foreland basin system.

Crustal thickness budgets calculated from our shortening estimates can account for 90%–104% of the crustal area of the retroarc observed today, assuming an initial crustal thickness of 35 km, but may have produced 2%–18% excess area for initial crustal thickness of 40 km, indicating the possibility of crustal flow or delamination at 21°S.

The locus of crustal thickening was likely beneath the EC and Altiplano. For an initial crustal thickness of 35 km, the predicted crustal thicknesses for the EC and Altiplano match present-day observed thicknesses, but were not achieved until the present. For a 40-km-thick initial crust, the modern observed thicknesses of the EC and Altiplano may have been achieved by ca. 10 Ma, and exceeded modern thicknesses by ~2.5–14.5 km by the present, suggesting crustal losses significant enough to have affected the surface elevation of the hinterland.

ACKNOWLEDGMENTS

This work was funded by National Science Foundation grant EAR-1250510 to Long and Horton. We thank Ramiro Matos for assistance with logistics, and Javier Matos for driving, translating, logistics, and assistance in the field. Constructive reviews from Richard Allmendinger and Nathan Eichelberger significantly improved this manuscript.

REFERENCES CITED

Allmendinger, R.W., and Gubbels, T., 1996, Pure and simple shear plateau uplift, Altiplano-Puna, Argentina and Bolivia: Tectonophysics, v. 259, p. 1–13, doi:10.1016/0040-1951(96)00024-8.

Allmendinger, R.W., and Judge, P.A., 2013, Stratigraphic uncertainty and errors in shortening from balanced sections in the North American Cordillera: Geological Society of America Bulletin, v. 125, p. 1569–1579, doi:10.1130/B30871.1.

Allmendinger, R.W., and Zapata, T.R., 2000, The footwall ramp of the Subandean decollement, northernmost Argentina, from extended correlation of seismic reflection data: Tectonophysics, v. 321, p. 37–55, doi:10.1016/S0040-1951(00)00077-9.

Allmendinger, R.W., Ramos, V.A., Jordan, T.E., Palma, M., and Isacks, B.L., 1983, Paleography and Andean structural geometry, northwest Argentina: Tectonics, v. 2, p. 1–16, doi:10.1029/TC002i001p00001.

Allmendinger, R.W., Jordan, T.E., Kay, S.M., and Isacks, B.L., 1997, Altiplano-Puna Plateau of the Central Andes: Annual Review of Earth and Planetary Sciences, v. 25, p. 139–174, doi:10.1146/annurev.earth.25.1.139.

ANCORP Working Group, 2003, Seismic imaging of a convergent continental margin and plateau in the central Andes (Andean Continental Research Project 1996): Journal of Geophysical Research, v. 108, 2328, doi:10.1029/2002JB001771.

Arriagada, C., Roperch, P., Mpodozis, C., and Cobbold, P.R., 2008, Paleogene building of the Bolivian orocline: Tectonic restoration of the central Andes in 2-D map view: Tectonics, v. 27, TC6014, doi:10.1029/2008TC002269.

Baby, P., Hérail, G., Salinas, R., and Sempere, T., 1992, Geometry and kinematic evolution of passive roof duplexes deduced from cross section balancing: Example from the foreland thrust system of the southern Bolivian Subandean: Tectonics, v. 11, p. 523–536, doi:10.1029/91TC03090.

Baby, P., Rochat, P., Mascle, G., and Hérail, G., 1997, Neogene shortening contribution to crustal thickening in the back arc of the Central Andes: Geology, v. 25, p. 883–886, doi:10.1130/0091-7613(1997)025<0883:NSCTCT>2.3.CO;2.

Barnes, J.B., and Ehlers, T.A., 2009, End member models for Andean Plateau uplift: Earth-Science Reviews, v. 97, p. 105–132, doi:10.1016/j.earscirev.2009.08.003.

Barnes, J.B., Ehlers, T.A., McQuarrie, N., O'Sullivan, P.B., and Tawackoli, S., 2008, Thermochronometer record of central Andean Plateau growth, Bolivia (19.5°S): Tectonics, v. 27, TC3003, doi:10.1029/2007TC002174.

Barnes, J.B., Ehlers, T.A., Insel, N., McQuarrie, N., and Poulsen, C.J., 2012, Linking orography, climate, and exhumation across the central Andes: Geology, v. 40, p. 1135–1138, doi:10.1130/G33229.1.

Baumont, D., Paul, A., Zandt, G., Beck, S.L., and Pederson, H., 2002, Lithospheric structure of the central Andes based on surface wave dispersion: Journal of Geophysical Research, v. 107, 2371, doi:10.1029/2001JB000345.

Beck, S.L., and Zandt, G., 2002, The nature of orogenic crust in the central Andes: Journal of Geophysical Research, v. 107, 2230, doi:10.1029/2000JB000124.

Beck, S.L., Zandt, G., Myers, S.C., Wallace, T.C., Silver, P.G., and Drake, L., 1996, Crustal-thickness variations in the central Andes: Geology, v. 24, p. 407–410, doi:10.1130/0091-7613(1996)024<0407.

Bertrand, H., Fornari, M., Marzoli, A., García-Duarte, R., and Sempere, T., 2014, The Central Atlantic Magmatic Province extends into Bolivia: Lithos, v. 188, p. 33–43, doi:10.1016/j.lithos.2013.10.019.

Boyer, S., 1995, Sedimentary basin taper as a factor controlling the geometry and advance of thrust belts: American Journal of Science, v. 295, p. 1220–1254, doi:10.2475/ajs.295.10.1220.

Boyer, S.E., and Elliott, D., 1982, Thrust systems: American Association of Petroleum Geologists Bulletin, v. 66, p. 1196–1230.

Brooks, B.A., et al., 2011, Orogenic-wedge deformation and potential for great earthquakes in the central Andean backarc: Nature Geoscience, v. 4, p. 380–383, doi:10.1038/ngeo1143.

Cadena, E.A., Anaya, F., and Croft, D.A., 2015, Giant fossil tortoise and freshwater chelid turtle remains from the middle Miocene, Quebrada Honda, Bolivia: Evidence for lower paleoelevations for the southern Altiplano: Journal of South American Earth Sciences, v. 64, p. 190–198, doi:10.1016/j.jsames.2015.10.013.

Cladouhos, T.T., Allmendinger, R.W., Coira, B., and Farrar, E., 1994, Late Cenozoic deformation in the Central Andes: Fault kinematics from the northern Puna, northwestern Argentina and southwestern Bolivia: Journal of South American Earth Sciences, v. 7, p. 209–228, doi:10.1016/0895-9811(94)90008-6.

Coney, P.J., and Evenchick, C.A., 1994, Consolidation of the American Cordilleras: Journal of South American Earth Sciences, v. 7, p. 241–262, doi:10.1016/0895-9811(94)90011-6.

Costa, C.H., Audemard, F.A.M., Bezerra, F.H.R., Lavenu, A., Machette, M.N., and París, G., 2006, An overview of the main Quaternary deformation of South America: Revista de la Asociación Geológica Argentina, v. 61, p. 461–479.

Coutand, I., Cobbold, P.R., De Urreiztieta, M., Gautier, P., Chauvin, A., Gapais, D., Rossello, E.A., and Lopez-Gamundi, O., 2001, Style and history of Andean deformation, Puna Plateau, northwestern Argentina: Tectonics, v. 20, p. 210–234, doi:10.1029/2000TC900031.

Dahlstrom, C.D.A., 1969, Balanced cross-sections: Canadian Journal of Earth Sciences, v. 6, p. 743–757.

Davis, D., Suppe, J., and Dahlen, F., 1983, Mechanics of fold-and-thrust belts and accretionary wedges: Journal of Geophysical Research, v. 88, p. 1153–1172, doi:10.1029/JB088iB02p01153.
DeCelles, P.G., and DeCelles, P.C., 2001, Rates of shortening, propagation, underthrusting, and flexural wave migration in continental orogenic systems: Geology, v. 29, p. 135–138, doi:10.1130/0091-7613(2001)029<0135:ROSPUA>2.0.CO;2.
DeCelles, P.G., and Horton, B.K., 2003, Early to middle Tertiary foreland basin development and the history of Andean crustal shortening in Bolivia: Geological Society of America Bulletin, v. 115, p. 58–77, doi:10.1130/0016-7606(2003)115<0058:ETMTFB>2.0.CO;2.
Decelles, P.G., and Mitra, G., 1995, History of the Sevier orogenic wedge in terms of critical taper models, northeast Utah and southwest Wyoming: Geological Society of America Bulletin, v. 107, p. 454–462, doi:10.1130/0016-7606(1995)107<0454:HOTSOW>2.3.CO;2.
DeCelles, P.G., Ducea, M.N., Kapp, P., and Zandt, G., 2009, Cyclicity in cordilleran orogenic systems: Nature Geoscience, v. 2, p. 251–257, doi:10.1038/ngeo469.
DeCelles, P.G., Zandt, G., Beck, S.L., Currie, C.A., Ducea, M.N., Kapp, P., Gehrels, G.E., Carrapa, B., Quade, J., and Schoenbohm, L.M., 2015, Cyclical orogenic processes in the Cenozoic central Andes, *in* DeCelles, P.G., et al., eds., Geodynamics of a Cordilleran Orogenic System: The Central Andes of Argentina and Northern Chile: Geological Society of America Memoir 212, p. 459–490, doi:10.1130/2015.1212(22).
Dorbath, C., Granet, M., Poupinet, G., and Martinez, C., 1993, A teleseismic study of the Altiplano and the Eastern Cordillera in northern Bolivia: New constraints on a lithospheric model: Journal of Geophysical Research, v. 98, p. 9825–9844, doi:10.1029/92JB02406.
Ducea, M.N., 2001, The California arc: Thick granitic batholiths, eclogitic residues, lithospheric-scale thrusting, and magmatic flare-ups: GSA Today, v. 11, no. 11, p. 4–10, doi:10.1130/1052-5173(2001)011<0004:TCATGB>2.0.CO;2.
Dunn, J., Hartshorn, K., and Hartshorn, P., 1995, Structural styles and hydrocarbon potential of the sub-Andean thrust belt of southern Bolivia, *in* Tankard, A.J., et al., eds., Petroleum Basins of South America: American Association of Petroleum Geologists Memoir 62, p. 523–543.
Echavarria, L., Hernández, R., Allmendinger, R., and Reynolds, J., 2003, Subandean thrust and fold belt of northwestern Argentina: Geometry and timing of the Andean evolution: American Association of Petroleum Geologists Bulletin, v. 87, p. 965–985, doi:10.1306/01200300196.
Ege, H., Sobel, E.R., Scheuber, E., and Jacobshagen, V., 2007, Exhumation history of the southern Altiplano plateau (southern Bolivia) constrained by apatite fission track thermochronology: Tectonics, v. 26, TC1004, doi:10.1029/2005TC001869.
Egenhoff, S.O., 2007, Life and death of a Cambrian–Ordovician basin: An Andean three-act play featuring Gondwana and the Arequipa-Antofalla terrane, *in* Linnemann, U., et al., eds., The Evolution of the Rheic Ocean: From Avalonian-Cadomian Active Margin to Alleghenian-Variscan Collision: Geological Society of America Special Paper 423, p. 511–524, doi:10.1130/2007.2423(26).
Eichelberger, N., and McQuarrie, N., 2015, Kinematic reconstruction of the Bolivian orocline: Geosphere, v. 11, p. 445–462, doi:10.1130/GES01064.1.
Eichelberger, N., McQuarrie, N., Ehlers, T.A., Enkelmann, E., Barnes, J.B., and Lease, R.O., 2013, New constraints on the chronology, magnitude, and distribution of deformation within the central Andean orocline: Tectonics, v. 32, p. 1432–1453, doi:10.1002/tect.20073.
Eichelberger, N., McQuarrie, N., Ryan, J., Karimi, B., Beck, S., and Zandt, G., 2015, Evolution of crustal thickening in the central Andes, Bolivia: Earth and Planetary Science Letters, v. 426, p. 191–203, doi:10.1016/j.epsl.2015.06.035.
Elger, K., Oncken, O., and Glodny, J., 2005, Plateau-style accumulation of deformation: Southern Altiplano: Tectonics, v. 24, TC4020, doi:10.1029/2004TC001675.
Elliott, D., 1983, The construction of balanced cross sections: Journal of Structural Geology, v. 5, 101, doi:10.1016/0191-8141(83)90035-4.
Erdos, Z., Huismans, R., and van der Beek, P., 2015, First-order control of syntectonic sedimentation on crustal-scale structure of mountain belts: Journal of Geophysical Research, v. 120, p. 5362–5377, doi:10.1002/2014JB011785.
Garzione, C.N., Molnar, P., Libarkin, J.C., and MacFadden, B.J., 2006, Rapid late Miocene rise of the Bolivian Altiplano: Evidence for removal of mantle lithosphere: Earth and Planetary Science Letters, v. 241, p. 543–556, doi:10.1016/j.epsl.2005.11.026.
Garzione, C.N., Hoke, G.D., Libarkin, J.C., Withers, S., MacFadden, B., Eiler, J., Ghosh, P., and Mulch, A., 2008, Rise of the Andes: Science, v. 320, p. 1304–1307, doi:10.1126/science.1148615.
Garzione, C.N., Auerbach, D.J., Jin-Sook Smith, J., Rosario, J.J., Passey, B.H., Jordan, T.E., and Eiler, J.M., 2014, Clumped isotope evidence for diachronous surface cooling of the Altiplano and pulsed surface uplift of the Central Andes: Earth and Planetary Science Letters, v. 393, p. 173–181, doi:10.1016/j.epsl.2014.02.029.
Gephart, J.W., 1994, Topography and subduction geometry in the Central Andes: Clues to the mechanics of a noncollisional orogen: Journal of Geophysical Research, v. 99, p. 12279–12288, doi:10.1029/94JB00129.
Ghosh, P., Garzione, C.N., and Eiler, J.M., 2006, Rapid uplift of the Altiplano revealed through ^{13}C–^{18}O bonds in paleosol carbonates: Science, v. 311, p. 511–515, doi:10.1126/science.1119365.
Gotberg, N., McQuarrie, N., and Caillaux, V.C., 2010, Comparison of crustal thickening budget and shortening estimates in southern Peru (12–14 S): Implications for mass balance and rotations in the "Bolivian orocline": Geological Society of America Bulletin, v. 122, p. 727–742, doi:10.1130/B26477.1.
Götze, H.J., Lahmeyer, B., Schmidt, S., and Strunk, S., 1994, The lithospheric structure of the Central Andes (20–25°S) as inferred from quantitative interpretation of regional gravity, *in* Reutter, K.J., et al., eds., Tectonics of the Southern Central Andes: Berlin, Springer, p. 7–22.
Gubbels, T., Isacks, B., and Farrar, E., 1993, High-level surfaces, plateau uplift, and foreland development, Bolivian central Andes: Geology, v. 21, p. 695–698, doi:10.1130/0091-7613(1993)021<0695:HLSPUA>2.3.CO;2.
Hatcher, R.D., and Hooper, R.J., 1992, Evolution of crystalline thrust sheet in the internal parts of mountain chains, *in* McClay, K.R., ed., Thrust Tectonics: New York, Chapman and Hall, p. 217–233, doi:10.1007/978-94-011-3066-0_20.
Hérail, G., Oller, J., Baby, P., Bonhomme, M., and Soler, P., 1996, Strike-slip faulting, thrusting and related basins in the Cenozoic evolution of the southern branch of the Bolivian orocline: Tectonophysics, v. 259, p. 201–212, doi:10.1016/0040-1951(95)00108-5.
Hindle, D., Kley, J., Oncken, O., and Sobolev, S., 2005, Crustal balance and crustal flux from shortening estimates in the Central Andes: Earth and Planetary Science Letters, v. 230, p. 113–124, doi:10.1016/j.epsl.2004.11.004.
Hoke, G.D., and Garzione, C.N., 2008, Paleosurfaces, paleoelevation, and the mechanisms for the late Miocene topographic development of the Altiplano plateau: Earth and Planetary Science Letters, v. 271, p. 192–201, doi:10.1016/j.epsl.2008.04.008.
Horton, B., 1999, Erosional control on the geometry and kinematics of thrust belt development in the central Andes: Tectonics, v. 18, p. 1292–1304, doi:10.1029/1999TC900051.
Horton, B., 2000, Sediment accumulation on top of the Andean orogenic wedge: Oligocene to late Miocene basins of the Eastern Cordillera, southern Bolivia: Reply: Geological Society of America Bulletin, v. 112, p. 1756–1759, doi:10.1130/0016-7606(2000)112<1756:R>2.0.CO;2.
Horton, B.K., 1998, Sediment accumulation on top of the Andean orogenic wedge: Oligocene to late Miocene basins of the Eastern Cordillera, southern Bolivia: Geological Society of America Bulletin, v. 110, p. 1174–1192, doi:10.1130/0016-7606(1998)110<1174:SAOTOT>2.3.CO;2.
Horton, B.K., 2005, Revised deformation history of the central Andes: Inferences from Cenozoic foredeep and intermontane basins of the Eastern Cordillera, Bolivia: Tectonics, v. 24, TC3011, doi:10.1029/2003TC001619.
Horton, B.K., and DeCelles, P.G., 1997, The modern foreland basin system adjacent to the Central Andes: Geology, v. 25, p. 895–898, doi:10.1130/0091-7613(1997)025<0895:TMFBSA>2.3.CO;2.
Horton, B.K., Hampton, B.A., and Waanders, G.L., 2001, Paleogene synorogenic sedimentation in the Altiplano plateau and implications for initial mountain building in the central Andes: Geological Society of America Bulletin, v. 113, p. 1387–1400, doi:10.1130/0016-7606(2001)113<1387:PSSITA>2.0.CO;2.
Hulka, C., and Heubeck, C., 2010, Composition and provenance history of late Cenozoic sediments in southeastern Bolivia: Implications for Chaco foreland basin evolution and Andean uplift: Journal of Sedimentary Research, v. 80, p. 288–299, doi:10.2110/jsr.2010.029.
Husson, L., and Sempere, T., 2003, Thickening the Altiplano crust by gravity-driven crustal channel flow: Geophysical Research Letters, v. 30, 1243, doi:10.1029/2002GL016877.
Isacks, B., 1988, Uplift of the central Andean plateau and bending of the Bolivian orocline: Journal of Geophysical Research, v. 93, p. 3211–3231, doi:10.1029/JB093iB04p03211.
Jacobshagen, V., Müller, J., Wemmer, K., Ahrendt, H., and Manutsoglu, E., 2002, Hercynian deformation and metamorphism in the Cordillera Oriental of southern Bolivia, central Andes: Tectonophysics, v. 345, p. 119–130, doi:10.1016/S0040-1951(01)00209-8.
Judge, P.A., and Allmendinger, R.W., 2011, Assessing uncertainties in balanced cross sections: Journal of Structural Geology, v. 33, p. 458–467, doi:10.1016/j.jsg.2011.01.006.
Kay, R.W., and Kay, S., 1993, Delamination and delamination magmatism: Tectonophysics, v. 219, p. 177–189, doi:10.1016/0040-1951(93)90295-U.

Kennan, L., Lamb, S., and Rundle, C., 1995, K-Ar dates from the Altiplano and Cordillera Oriental of Bolivia: Implications for Cenozoic stratigraphy and tectonics: Journal of South American Earth Sciences, v. 8, p. 163–186, doi:10.1016/0895-9811(95)00003-X.

Kennan, L., Lamb, S.H., and Hoke, L., 1997, High-altitude palaeosurfaces in the Bolivian Andes: Evidence for late Cenozoic surface uplift, *in* Widdowson, M., ed., Palaeosurfaces: Recognition, Reconstruction and Palaeoenvironmental Interpretation: Geological Society of London Special Publication 120, p. 307–323, doi:10.1144/GSL.SP.1997.120.01.20.

Kley, J., 1996, Transition from basement-involved to thin-skinned thrusting in the Cordillera Oriental of southern Bolivia: Tectonics, v. 15, p. 763–775, doi:10.1029/95TC03868.

Kley, J., 1999, Geologic and geometric constraints on a kinematic model of the Bolivian orocline: Journal of South American Earth Sciences, v. 12, p. 221–235, doi:10.1016/S0895-9811(99)00015-2.

Kley, J., and Monaldi, C.R., 1998, Tectonic shortening and crustal thickness in the Central Andes: How good is the correlation?: Geology, v. 26, p. 723–726, doi:10.1130/0091-7613(1998)026<0723:TSACTI>2.3.CO;2.

Kley, J., and Monaldi, C.R., 2002, Tectonic inversion in the Santa Barbara System of the central Andean foreland thrust belt, northwestern Argentina: Tectonics, v. 21, 1061, doi:10.1029/2002TC902003.

Kley, J., Gangui, A.H., and Kruger, D., 1996, Basement-involved blind thrusting in the eastern Cordillera Oriental, southern Bolivia: Evidence from cross sectional balancing, gravimetric and magnetotelluric data: Tectonophysics, v. 259, p. 171–184, doi:10.1016/0040-1951(95)00067-4.

Kley, J., Muller, J., Tawackoli, S., Jacobshagen, V., and Manutsoglu, E., 1997, Pre-Andean and Andean-age deformation in the Eastern Cordillera of southern Bolivia: Journal of South American Earth Sciences, v. 10, p. 1–19, doi:10.1016/S0895-9811(97)00001-1.

Kley, J., Monaldi, C.R., and Salfity, J.A., 1999, Along-strike segmentation of the Andean foreland: Causes and consequences: Tectonophysics, v. 301, p. 75–94, doi:10.1016/S0040-1951(98)90223-2.

Krystopowicz, N.J., and Currie, C.A., 2013, Crustal eclogitization and lithosphere delamination in orogens: Earth and Planetary Science Letters, v. 361, p. 195–207, doi:10.1016/j.epsl.2012.09.056.

Lallemand, S., Heuret, A., and Boutelier, D., 2005, On the relationships between slab dip, back-arc stress, upper plate absolute motion, and crustal nature in subduction zones: Geochemistry, Geophysics, Geosystems, v. 6, Q09006, doi:10.1029/2005GC000917.

Lamb, S., and Hoke, L., 1997, Origin of the high plateau in the Central Andes, Bolivia, South America: Tectonics, v. 16, p. 623–649, doi:10.1029/97TC00495.

Lucassen, F., Lewerenz, S., Franz, G., Viramonte, J., and Mezger, K., 1999, Metamorphism, isotopic ages and composition of lower crustal granulite xenoliths from the Cretaceous Salta Rift, Argentina: Contributions to Mineralogy and Petrology, v. 134, p. 325–341, doi:10.1007/s004100050488.

Lyon-Caen, H., Molnar, P., and Suarez, G., 1985, Gravity anomalies and flexure of the Brazilian shield beneath the Bolivian Andes: Earth and Planetary Science Letters, v. 75, p. 81–92, doi:10.1016/0012-821X(85)90053-6.

Malavieille, J., 2010, Impact of erosion, sedimentation, and structural heritage on the structure and kinematics of orogenic wedges: Analog models and case studies: GSA Today, v. 20, no. 1, p. 4–10, doi:10.1130/GSATG48A.1.

McGroder, M.F., Lease, R.O., and Pearson, D.M., 2015, Along-strike variation in structural styles and hydrocarbon occurrences, Subandean fold-and-thrust belt and inner foreland, Colombia to Argentina, *in* DeCelles, P.G., et al., eds., Geodynamics of a Cordilleran Orogenic System: The Central Andes of Argentina and Northern Chile: Geological Society of America Memoir 212, p. 79–113, doi:10.1130/2015.1212(05).

McQuarrie, N., 2002, The kinematic history of the central Andean fold-thrust belt, Bolivia: Implications for building a high plateau: Geological Society of America Bulletin, v. 114, p. 950–963, doi:10.1130/0016-7606(2002)114<0950.

McQuarrie, N., and DeCelles, P., 2001, Geometry and structural evolution of the central Andean backthrust belt, Bolivia: Tectonics, v. 20, p. 669–692, doi:10.1029/2000TC001232.

McQuarrie, N., Horton, B.K., Zandt, G., Beck, S., and DeCelles, P.G., 2005, Lithospheric evolution of the Andean fold–thrust belt, Bolivia, and the origin of the central Andean plateau: Tectonophysics, v. 399, p. 15–37, doi:10.1016/j.tecto.2004.12.013.

McQuarrie, N., Ehlers, T.A., Barnes, J.B., and Meade, B., 2008a, Temporal variation in climate and tectonic coupling in the central Andes: Geology, v. 36, p. 999–1002, doi:10.1130/G25124A.1.

McQuarrie, N., Barnes, J.B., and Ehlers, T.A., 2008b, Geometric, kinematic, and erosional history of the central Andean Plateau, Bolivia (15–17°S): Tectonics, v. 27, TC3007, doi:10.1029/2006TC002054.

Mingramm, A., Russo, A., Pozzo, A., and Cazau, L., 1979, Sierras Subandianas, *in* Segundo Simposio de Geología Regional Argentina: Cordoba, Argentina, Academia Nacional de Ciencias, v. 1, p. 95–138.

Mitra, G., 1978, Ductile deformation zones and mylonites: The mechanical processes involved in the deformation of crystalline basement rocks: American Journal of Science, v. 278, p. 1057–1084, doi:10.2475/ajs.278.8.1057.

Molnar, P., and Garzione, C.N., 2007, Bounds on the viscosity coefficient of continental lithosphere from removal of mantle lithosphere beneath the Altiplano and Eastern Cordillera: Tectonics, v. 26, TC201, doi:10.1029/2006TC001964.

Mon, R., and Hongn, F., 1991, The structure of the Precambrian and lower Paleozoic basement of the Central Andes between 22° and 32° S Lat: Geologische Rundschau, v. 80, p. 745–758, doi:10.1007/BF01803699.

Montgomery, D., Balco, G., and Willett, S., 2001, Climate, tectonics, and the morphology of the Andes: Geology, v. 29, p. 579–582, doi:10.1130/0091-7613(2001)029<0579:CTATMO>2.0.CO;2.

Moretti, I., Baby, P., Mendez, E., and Zubieta, D., 1996, Hydrocarbon generation in relation to thrusting in the Sub Andean zone from 18 to 22 degrees S, Bolivia: Petroleum Geoscience, v. 2, p. 17–28, doi:10.1144/petgeo.2.1.17.

Mugnier, J.L., Becel, D., and Granjeon, D., 2006, Active tectonics in the Subandean belt inferred from the morphology of the Rio Pilcomayo (Bolivia), *in* Willett, S.D., et al., eds., Tectonics, Climate, and Landscape Evolution: Geological Society of America Special Paper 398, p. 353–369, doi:10.1130/2006.2398(22).

Müller, J.P., Kley, J., and Jacobshagen, V., 2002, Structure and Cenozoic kinematics of the Eastern Cordillera, southern Bolivia (21°S): Tectonics, v. 21, 1037, doi:10.1029/2001TC001340.

Oncken, O., Hindle, D., Kley, J., Elger, K., Victor, P., and Schemmann, K., 2006, Deformation of the Central Andean upper plate system—Facts, fiction, and constraints for plateau models, *in* Oncken, O., et al., eds., The Andes—Active Subduction Orogeny: Frontiers in Earth Sciences: Berlin, Springer, p. 3–27, doi:10.1007/978-3-540-48684-8_1.

Pardo Casas, F., and Molnar, P., 1987, Relative motion of the Nazca (Farallon) and South American plates since Late Cretaceous time: Tectonics, v. 6, p. 233–248, doi:10.1029/TC006i003p00233.

Pearson, D.M., Kapp, P., DeCelles, P.G., Reiners, P.W., Gehrels, G.E., Ducea, M.N., and Pullen, A., 2013, Influence of pre-Andean crustal structure on Cenozoic thrust belt kinematics and shortening magnitude: Northwestern Argentina: Geosphere, v. 9, p. 1766–1782, doi:10.1130/GES00923.1.

Perez, N.D., Horton, B.K., McQuarrie, N., Stubner, K., and Ehlers, T.A., 2016, Andean shortening, inversion and exhumation associated with thin- and thick-skinned deformation in southern Peru: Geological Magazine, v. 153, p. 1013–1041, doi:10.1017/S0016756816000121.

Prezzi, C.B., Uba, C.E., and Götze, H.-J., 2009, Flexural isostasy in the Bolivian Andes: Chaco foreland basin development: Tectonophysics, v. 474, p. 526–543, doi:10.1016/j.tecto.2009.04.037.

Profeta, L., Ducea, M.N., Chapman, J.B., Paterson, S.R., Gonzales, S.M.H., Kirsch, M., Petrescu, L., and DeCelles, P.G., 2015, Quantifying crustal thickness over time in magmatic arcs: Scientific Reports, v. 5, 17786, doi:10.1038/srep17786.

Salfity, J.A., and Marquillas, R.A., 1994, Tectonic and sedimentary evolution of the Cretaceous–Eocene Salta Group basin, Argentina, *in* Salfity, J.A., ed., Cretaceous Tectonics of the Andes: Wiesbaden, Germany, Vieweg Publishing, p. 266–315.

Schmitz, M., 1994, A balanced model of the southern Central Andes: Tectonics, v. 13, p. 484–492, doi:10.1029/93TC02232.

Schmitz, M., and Kley, J., 1997, The geometry of the central Andean backarc crust: Joint interpretation of cross section balancing and seismic refraction data: Journal of South American Earth Sciences, v. 10, p. 99–110, doi:10.1016/S0895-9811(97)00009-6.

Sempere, T., 1994, Kimmeridgian? to Paleocene tectonic evolution of Bolivia, *in* Salfity, J.A., ed., Cretaceous Tectonics of the Andes: Earth Evolution Sciences Monograph: Wiesbaden, Vieweg+Teubner Verlag, p. 168–212, doi:10.1007/978-3-322-85472-8_4.

Sempere, T., 1995, Phanerozoic evolution of Bolivia and adjacent regions, *in* Tankard, A.J., et al., eds., Petroleum Basins of South America: American Association of Petroleum Geologists Memoir 62, p. 207–230.

Sempere, T., 2000, Sediment accumulation on top of the Andean orogenic wedge: Oligocene to late Miocene basins of the Eastern Cordillera, southern Bolivia: Discussion and Reply: Geological Society of America Bulletin, v. 112, p. 1752–1755, doi:10.1130/0016-7606(2000)112<1752:DSAOTO>2.0.CO;2.

Sempere, T., Butler, R.F., Richards, D.R., Marshall, L.G., Sharp, W., and Swisher, C.C., III, 1997, Stratigraphy and chronology of Upper Cretaceous–lower Paleogene strata in Bolivia and northwest Argentina: Geological Society of America Bulletin, v. 109, p. 709–727, doi:10.1130/0016-7606(1997)109<0709:SACOUC>2.3.CO;2.

Sempere, T., et al., 2002, Late Permian–Middle Jurassic lithospheric thinning in Peru and Bolivia, and its bearing on Andean-age tectonics: Tectonophysics, v. 345, p. 153–181, doi:10.1016/S0040-1951(01)00211-6.

Servicio Geologico de Bolivia, 1992, Mapas Tematicos de Recursos Minerales de Bolivia, Hojas Tarija y Villazon: La Paz, Servicio Geologico de Bolivia, serie II-MTB-1B, scale 1:250,000.

Servicio Nacional de Geologica y Tecnico de Minas, 2009, Carta Geologica de Bolivia, Hoja 6729 Entre Rios: La Paz, Servicio Geologica de Bolivia SGTM serie I–CGB-53, scale 1:100,000.

Servicio Nacional de Geologica y Tecnico de Minas, 2010, Carta Geologica de Bolivia, Hoja 6329 Chilcobija: La Paz, Servicio Nacional de Geologica y Tecnico de Minas, SGTM serie I–CGB-57, scale 1:100,000.

Sheffels, B.M., 1990, Lower bound on the amount of crustal shortening in the central Bolivian Andes: Geology, v. 18, p. 812–815, doi:10.1130/0091-7613(1990)018<0812:LBOTAO>2.3.CO;2.

Sobel, E., Hilley, G., and Strecker, M., 2003, Formation of internally drained contractional basins by aridity-limited bedrock incision: Journal of Geophysical Research, v. 108, 2344, doi:10.1029/2002JB001883.

Sobolev, S.V., and Babeyko, A.Y., 2005, What drives orogeny in the Andes?: Geology, v. 33, p. 617–620, doi:10.1130/G21557.1.

Tankard, A., et al., 1995, Structural and tectonic controls of basin evolution in southwestern Gondwana during the Phanerozoic, *in* Tankard, A.J., et al., eds., Petroleum Basins of South America: American Association of Petroleum Geologists Memoir 62, p. 5–52.

Uba, C.E., Heubeck, C., and Hulka, C., 2006, Evolution of the late Cenozoic Chaco foreland basin, southern Bolivia: Basin Research, v. 18, p. 145–170, doi:10.1111/j.1365-2117.2006.00291.x.

Uba, C.E., Kley, J., Strecker, M.R., and Schmitt, A.K., 2009, Unsteady evolution of the Bolivian Subandean thrust belt: The role of enhanced erosion and clastic wedge progradation: Earth and Planetary Science Letters, v. 281, p. 134–146, doi:10.1016/j.epsl.2009.02.010.

Wang, H., Currie, C.A., and DeCelles, P.G., 2015, Hinterland basin formation and gravitational instabilities in the central Andes: Constraints from gravity data and geodynamic models, *in* DeCelles, P.G., et al., eds., Geodynamics of a Cordilleran Orogenic System: The Central Andes of Argentina and Northern Chile: Geological Society of America Memoir 212, p. 387–406, doi:10.1130/2015.1212(19).

Wells, M.L., Hoisch, T.D., Cruz-Uribe, A.M., and Vervoort, J.D., 2012, Geodynamics of synconvergent extension and tectonic mode switching: Constraints from the Sevier-Laramide orogen: Tectonics, v. 31, p. 1–20, doi:10.1029/2011TC002913.

Welsink, H.J., A. Franco, M., and C. Oviedo, G., 1995, Andean and pre-Andean deformation, Boomerang Hills area, Bolivia, *in* Tankard, A.J., et al., eds., Petroleum Basins of South America: American Association of Petroleum Geologists Memoir 62, p. 481–499.

Wigger, P., et al., 1994, Variation in the crustal structure of the southern Central Andes deduced from seismic refraction investigations, *in* Reutter, L., et al., eds., Tectonics of the Southern Central Andes: New York, Springer-Verlag, p. 23–48, doi:10.1007/978-3-642-77353-2_2.

Willett, S.D., 1999, Orogeny and orography: The effects of erosion on the structure of mountain belts: Journal of Geophysical Research, v. 104, p. 28,957–28,981, doi:10.1029/1999JB900248.

Woodward, N.B., Boyer, S.E., and Suppe, J., 1989, Balanced Geological Cross sections: An Essential Technique in Geological Research and Exploration: American Geophysical Union Short Courses in Geology Volume 6, 132 p., doi:10.1029/SC006.

Yagupsky, D.L., Brooks, B.A., Whipple, K.X., Duncan, C.C., and Bevis, M., 2014, Distribution of active faulting along orogenic wedges: Minimum-work models and natural analogue: Journal of Structural Geology, v. 66, p. 237–247, doi:10.1016/j.jsg.2014.05.025.

Yuan, X., et al., 2000, Subduction and collision processes in the Central Andes constrained by converted seismic phases: Nature, v. 408, p. 958–961, doi:10.1038/35050073.